High and stable ATP levels prevent aberrant intracellular protein aggregation

Masak Takaine[1,2]*, Hiromi Imamura[3], Satoshi Yoshida[1,2,4,5]*

[1]Gunma University Initiative for Advanced Research (GIAR), Gunma University, Maebashi 371-8512, Japan

[2]Institute for Molecular and Cellular Regulation (IMCR), Gunma University, Maebashi 371-8512, Japan

[3]Graduate School of Biostudies, Kyoto University, Kyoto 606-8501, Japan

[4]School of International Liberal Studies, Waseda University, Tokyo, 169-8050, Japan

[5]Japan Science and Technology Agency, PREST

*Correspondence should be addressed to: masaktakaine@gunma-u.ac.jp (M.T.) (Lead contact) or satosh@waseda.jp (S.Y.)

Running title

ATP homeostasis prevents cytotoxic protein aggregation

Keywords

ATP, homeostasis, proteostasis, yeast, neurodegenerative disease, AMPK, adenylate kinase, protein aggregation

ABSTRACT

ATP at millimolar levels has recently been implicated in the solubilization of cellular proteins. However, the significance of this high ATP level under physiological conditions and the mechanisms that maintain ATP remain unclear. We herein demonstrated that AMP-activated protein kinase (AMPK) and adenylate kinase (ADK) cooperated to maintain cellular ATP levels regardless of glucose levels. Single cell imaging of ATP-reduced yeast mutants revealed that ATP levels in these mutants repeatedly underwent stochastic and transient depletion, which induced the cytotoxic aggregation of endogenous proteins and pathogenic proteins, such as huntingtin and α-synuclein. Moreover, pharmacological elevations in ATP levels in an ATP-reduced mutant prevented the accumulation of α-synuclein aggregates and its cytotoxicity. The removal of cytotoxic aggregates depended on proteasomes, and proteasomal activity cooperated with AMPK or ADK to resist proteotoxic stresses. The present study is the first to demonstrate that cellular ATP homeostasis ensures proteostasis and revealed that suppressing the high volatility of cellular ATP levels prevented cytotoxic protein aggregation, implying that AMPK and ADK are important factors that prevent proteinopathies, such as neurodegenerative diseases.

INTRODUCTION

Adenosine triphosphate (ATP) is the main energy currency used by all living organisms. In addition to its role as energy currency, ATP has recently been suggested to influence the balance between the soluble and aggregated states of proteins, indicating that proteostasis is maintained by energy-dependent chaperones and also by the property of ATP as a hydrotrope to solubilize proteins (Hayes, Peuchen et al., 2018, Patel, Malinovska et al., 2017, Pu, Li et al., 2019, Sridharan, Kurzawa et al., 2019). Furthermore, ATP levels have been shown to regulate the physicochemical properties of the cytoplasm, such as viscosity, macromolecular crowding, and liquid-liquid phase separation (Marini, Nuske et al., 2020, Persson, Ambati et al., 2020). However, the role of ATP was assessed in these studies using artificial ATP depletion. Therefore, it currently remains unclear whether ATP-dependent protein solubilization/desolubilization have physiologically significant cellular roles.

We recently established a reliable imaging technique to quantify intracellular ATP levels in single living yeast cells using the genetically encoded fluorescent ATP biosensor QUEEN (Yaginuma, Kawai et al., 2014), which enables long-term evaluations of ATP homeostasis in individual cells (Takaine, Ueno et al., 2019). The findings obtained demonstrated that intracellular ATP levels did not vary within a yeast population grown in the same culture (Takaine et al., 2019), which was in contrast to the large variations observed in intracellular ATP levels within a bacterial cell population (Yaginuma et al., 2014). Moreover, intracellular ATP levels in individual living yeast cells were stably and robustly maintained at approximately 4 mM, irrespective of carbon sources and cell cycle stages, and temporal fluctuations in intracellular ATP levels were small (Takaine et al., 2019). Based on these findings, we hypothesized that an exceptionally robust mechanism exists to precisely regulate ATP levels in eukaryotes. It currently remains unclear why ATP is stably maintained at a markedly higher level than the K_m (Michaelis constant) required for the enzymatic activities of most ATPases (Edelman, Blumenthal et al., 1987), and the consequences associated with failed ATP homeostasis in living organisms have not yet been elucidated.

The most promising candidate regulator of ATP homeostasis is AMP-activated protein kinase (AMPK). AMPK, which is activated by AMP and inhibited by ATP (Xiao, Heath et al., 2007), has long been regarded as an important regulator of the whole-body and cellular energy status in eukaryotes (Hardie, Schaffer et al., 2016). AMPK is activated by increases in the AMP:ATP or ADP:ATP ratio (*i.e.,* low-energy state), and regulates its downstream effectors by phosphorylation to redirect cell metabolism from an anabolic (ATP-consuming) state to

73 catabolic (ATP-producing) state (Herzig & Shaw, 2017). In the budding yeast *Saccharomyces*
74 *cerevisiae*, the sucrose non-fermenting 1 (Snf1) protein kinase complex is the sole AMPK.
75 Similar to other AMPKs, the yeast Snf1 complex comprises three subunits: the catalytic α
76 subunit (*SNF1*), scaffolding β subunit (*SIP1*, *SIP2* or *GAL83*), and regulatory γ subunit
77 (*SNF4*) (Ghillebert, Swinnen et al., 2011). The role of the Snf1 complex in adaptation to
78 glucose limitations has been characterized in detail (Hedbacker & Carlson, 2008). The Snf1
79 complex is inactive in the presence of sufficient glucose levels in media (Wilson, Hawley et
80 al., 1996). Decreases in glucose levels have been shown to activate the Snf1 complex and
81 phosphorylate the transcriptional repressor Mig1, which then triggers the transcription of
82 numerous glucose-repressed genes (Carlson, 1999). However, the contribution of AMPK or
83 the Snf1 complex to cellular ATP levels remains unknown.
84
85 Other possible candidate regulators of ATP homeostasis include genes whose mutation leads
86 to decreases in the cellular content of ATP. However, based on biochemical analyses of cell
87 populations, few yeast mutants reduced ATP levels (Gauthier, Coulpier et al., 2008,
88 Ljungdahl & Daignan-Fornier, 2012). Adenylate kinase (ADK) is a key enzyme that
89 synthesizes ATP and AMP using two ADP molecules as substrates, and the null mutant of
90 ADK (*adk1*Δ) was shown to have a reduced cellular ATP level (~70% of the wild type)
91 (Gauthier et al., 2008). Bas1 is a transcription factor that is required for *de novo* purine
92 synthesis and *bas1*Δ also has a reduced ATP level (~50% of the wild type) (Gauthier et al.,
93 2008). However, the regulation of ATP levels and the physiological consequences of reduced
94 ATP levels in these mutants remain unclear, particularly at the single cell level.
95
96 In the present study, we investigated the roles of AMPK, ADK, and Bas1 in ATP homeostasis
97 using the QUEEN-based single cell ATP imaging technique. We demonstrated for the first
98 time that AMPK is involved in the regulation of intracellular ATP levels, even under
99 glucose-rich conditions. Furthermore, time-lapse ATP imaging revealed that cells lacking
100 both AMPK and ADK frequently underwent transient ATP depletion, while ATP levels
101 oscillated in those lacking Bas1. These ATP dynamics in the mutants were overlooked in
102 previous biochemical studies. We found that some intrinsic proteins and aggregation-prone
103 model proteins, including α-synuclein, which is responsible for Parkinson's disease,
104 aggregated and were cytotoxic in all of the ATP-reduced mutants tested. The present results
105 suggest that the stable maintenance of ATP is essential for proteostasis and imply that an ATP
106 crisis promotes proteinopathies, such as neurodegenerative diseases.

107 **RESULTS**

108 ADK1 cooperates with AMPK to regulate ATP homeostasis

109 We recently developed a reliable monitoring system for cytoplasmic ATP levels in living
110 yeast cells using the ATP biosensor QUEEN (Takaine et al., 2019). We herein conducted a
111 more detailed examination of ATP dynamics in wild-type and mutant yeast cells using this
112 system. We initially investigated whether the deletion of *SNF1*, which encodes a catalytic
113 subunit of AMPK, affected cellular ATP levels. Cellular ATP levels were significantly lower
114 in *SNF1*-null mutant (*snf1*Δ) cells than in wild-type cells at various glucose levels (Fig. 1A
115 and Fig. S1A, B). It is important to note that in addition to low glucose conditions (0.05%
116 glucose), at which the Snf1 complex is active, *snf1*Δ cells showed significantly reduced ATP
117 levels even under high glucose conditions (2% glucose), at which the Snf1 complex is
118 considered to be inactive. The deletion of *MIG1* had a negligible effect on ATP levels (Fig.
119 S1C), suggesting that as yet unknown factors other than Mig1 primarily regulate ATP levels
120 under the control of the Snf1 complex. Collectively, these results demonstrated for the first
121 time that AMPK/SNF1 affect cellular ATP levels even under glucose-rich conditions.

122

123 ADK catalyzes the interconversion of adenine nucleotides (ATP+AMP ⟷ 2ADP), which is
124 important for *de novo* adenine nucleotide synthesis and the balance between ATP, ADP, and
125 AMP. Previous biochemical studies reported that the deletion of the ADK gene reduced ATP
126 levels in mouse skeletal muscle cells and budding yeasts (Gauthier et al., 2008, Janssen,
127 Dzeja et al., 2000). We confirmed these findings using an ATP imaging method: *adk1*Δ cells
128 showed significantly lower QUEEN ratios than wild-type cells on average in the presence of
129 sufficient carbon sources (Fig. S2).

130

131 In addition to being a key enzyme in purine metabolism, ADK has also been suggested to
132 cooperate with AMPK in order to monitor the cellular energy state (Hardie, Carling et al.,
133 1998). Therefore, we compared ATP levels in *snf1*Δ *adk1*Δ double mutant cells with those in
134 *snf1*Δ, *adk1*Δ cells and wild-type cells (Fig. 1A, B). *snf1Δ adk1Δ* cells had significantly lower
135 average ATP levels than single mutant cells. We also found not only a general reduction, but
136 also a marked variation in ATP levels in the *snf1*Δ, *adk1Δ, snf1*Δ *adk1Δ* cell population, as
137 indicated by the large coefficient of variance (CV) (Fig. 1B). Furthermore, some *snf1Δ adk1Δ*
138 cells had very low ATP levels (Fig. 1A, B). These results suggest that Adk1 and the Snf1
139 complex both synergistically contribute to ATP homeostasis.

140

141 We confirmed the decreases observed in ATP levels in *snf1Δ*, *adk1Δ* and *snf1Δadk1Δ* cells

142 using a biochemical assay of whole cell extract (Fig. 1C). ADP levels were also reduced in
143 these mutant cells (Fig. S3). In *adk1Δ* cells, the ATP/ADP ratio increased, whereas the sum of
144 ATP and ADP levels decreased (Fig. S3), which is consistent with previous findings
145 (Gauthier et al., 2008). These biochemical data and their relevance to QUEEN data are
146 discussed later.
147

148 ## A large pool of adenine nucleotides is important for maintaining cellular ATP levels

149 We examined a *bas1Δ* mutant, which is defective in the expression of genes responsible for
150 adenine biogenesis (Daignan-Fornier & Fink, 1992, Denis, Boucherie et al., 1998). Consistent
151 with previous biochemical findings (Gauthier et al., 2008), ATP levels quantified by QUEEN
152 were reduced by ~50% in *bas1Δ* cells (Fig. 1D, E). We found not only a general reduction,
153 but also a marked variation in ATP levels in the *bas1Δ* cell population, as indicated by the
154 large CV (Fig. 1E). The decrease observed in ATP levels was due to reduced adenine
155 biosynthesis because the addition of extra adenine to media partially restored ATP levels (Fig.
156 1E). These results suggest that the sufficient production of adenine nucleotides is essential for
157 the stable maintenance of ATP levels. Moreover, the role of Bas1 in maintaining ATP levels
158 appeared to be epistatic to that of Snf1 because *bas1Δ snf1Δ* double mutant cells showed a
159 similar distribution of ATP levels to *bas1Δ* cells (Fig. S4). We confirmed the decrease
160 observed in ATP levels in *bas1Δ* cells using a biochemical assay (Fig. 1F). ADP levels and
161 the sum of ATP and ADP levels also significantly decreased in *bas1Δ* cells (Fig. S3), which is
162 consistent with previous findings (Gauthier et al., 2008).
163

164 ## ATP levels temporally fluctuate in ATP mutant cells

165 To investigate the mechanisms contributing to the marked variations in ATP levels in *snf1Δ*
166 *adk1Δ* cells in more detail, we employed time-lapse ATP imaging (Fig. 2). We found that the
167 QUEEN ratio often underwent a rapid decline followed by recovery in *snf1Δ adk1Δ* cells (see
168 116 and 132 min in Fig. 2A, C, and Movie S1, and 180 and 356 min in Fig. 2B, D, and Movie
169 S2). The sudden decrease in ATP levels (hereafter called "the ATP catastrophe") occurred
170 within a few minutes without any sign and was never observed in wild-type cells (Takaine et
171 al., 2019). The ATP catastrophe appeared to be a stochastic event and cell intrinsic: these
172 events occurred independent of the cell cycle stage or cell size (compare Fig. 2C with D).
173 Under some conditions, the QUEEN ratio did not recover after the ATP catastrophe and the
174 cell died, as judged by the loss of QUEEN signals in the cell (Fig. S5). These results suggest
175 that the marked variations observed in ATP levels in *snf1Δ adk1Δ* cells were not simply due
176 to a mixed population with different basal ATP levels, but were rather caused by the

177 stochastic ATP catastrophe in individual cells.
178
179 Time-lapse imaging of *bas1Δ* revealed oscillatory cycles in ATP levels (Figs. 2E and S6A,
180 and Movies S3 and S4): ATP cycling in *bas1Δ* cells was slow (~35 min on average, Fig. S6B)
181 and distinguishable from that in *snf1Δ adk1Δ* cells; however, the common characteristics of
182 these mutants were that the level of ATP repeatedly reached close to 0 mM. The ATP
183 oscillation cycle was unsynchronized in the population and independent of cell cycle
184 progression, suggesting a unique metabolic rhythm intrinsic to each cell. The oscillatory
185 nature of ATP cycling in the *bas1Δ* mutant may involve a transcription/translation cycle and
186 will be described elsewhere.
187
188 ATP homeostasis is required for preventing protein aggregation *in vivo*
189 We recently reported that cellular ATP levels were stably maintained at ~4 mM in budding
190 yeast (Takaine et al., 2019) and herein demonstrated that Adk1 and Bas1 in the Snf1/AMPK
191 complex were required for the regulation of ATP homeostasis. However, the physiological
192 importance of ATP homeostasis remains unknown. To clarify the significance of high ATP
193 levels, we examined the global genetic interactions of *snf1Δ*, *adk1Δ*, and *bas1Δ* using
194 CellMap ((Usaj, Tan et al., 2017), thecellmap.org). An *in silico* analysis identified genes
195 involved in "protein folding/glycosylation" as common negative genetic interactors with
196 *adk1Δ* and *bas1Δ* (Fig. 3A). Negative genetic interactors of *ura6*, a gene encoding uridylate
197 kinase that also exhibits ADK activity, were enriched in the "protein folding/glycosylation"
198 category (Fig. 3A). We also found that interactors of *snf1* were implicated in "protein
199 folding/glycosylation". None of these mutants exhibited apparent genetic interactions with
200 genes in the "metabolism" category (Fig. 3A). The same analysis using genetic and physical
201 interactors provided similar results and showed that many interactors were enriched in the
202 "protein turnover" category (Fig. S7). These results imply that although these three mutants
203 regulate ATP with distinct mechanisms, all three have a common cellular function.
204
205 To examine possible defects in protein folding and turnover (*i.e.*, proteostasis), we challenged
206 these mutants with various proteotoxic stresses. We found negligible growth defects in ATP
207 mutants under normal growth conditions with 2% glucose at 30°C (control in Fig. 3B),
208 suggesting that a high level of ATP is not necessary for cellular growth. However, the *adk1*
209 and *bas1* mutants both exhibited severe growth defects with a high temperature of 40°C, 1
210 hour of heat shock at 55°C, or in the presence of 0.5 μg/ml of the glycosylation inhibitor
211 tunicamycin or 2 mM H_2O_2. The *SNF1* deletion increased the stress sensitivity of *adk1Δ* (Fig.

212 3B). This sensitivity to proteotoxic stress suggests that ATP homeostasis mutants are
213 defective in some aspects of proteostasis. We found that all four mutants tested contained
214 significantly increased numbers of Hsp104-GFP foci, a marker of protein aggregation
215 (Josefson, Andersson et al., 2017) (Fig. 3C, D). In contrast to Hsp104-GFP foci, Pab1-GFP, a
216 marker of stress granule (SG) assembly (Hoyle, Castelli et al., 2007), did not form foci in
217 ATP mutants, suggesting that protein aggregation and SG assembly are regulated in a distinct
218 manner (Fig. 3D). These analyses identified abnormal protein aggregation as a common
219 defect associated with ATP homeostasis mutants for the first time.
220

221 ## The transient depletion of ATP leads to the formation of protein aggregates

222 To examine whether ATP depletion triggers protein aggregation in living yeast, we artificially
223 depleted cellular ATP levels by replacing glucose with 2-deoxyglucose (2DG), a strong
224 inhibitor of glycolysis, in media and monitored protein aggregation using Hsp104-GFP as a
225 marker of protein aggregation (Josefson et al., 2017) in wild-type cells. We previously
226 showed that ATP levels were almost completely depleted 2 minutes after the 2DG treatment
227 (Takaine et al., 2019), which was also confirmed biochemically (Fig. S3B). Within 15 min of
228 the 2DG treatment, more than 20% of cells contained Hsp104-GFP foci indicative of protein
229 aggregation (Fig. 4A, B). These protein aggregations were retained for hours after refeeding
230 of glucose (Fig. 4A, B), suggesting that the dissolution kinetics of Hsp104-GFP were
231 significantly slow. This contrasts intracellular ATP, which recovers to normal levels within 1
232 min of glucose refeeding (Takaine et al., 2019).
233

234 To further confirm whether a high level of ATP is required for protein solubility, we also
235 tested the Ubc9-ts protein, a model protein that is prone to aggregation (Kaganovich, Kopito
236 et al., 2008), and found that ATP depletion by the 2DG treatment triggered Ubc9-ts protein
237 aggregation (Fig. 4C). Therefore, not only Hsp104-GFP-positive intrinsic proteins, but also
238 extrinsic model proteins aggregate after ATP depletion.
239

240 SG are assembled in budding yeast cells under stress conditions, such as glucose depletion
241 (Hoyle et al., 2007). In contrast to the formation of Hsp104-GFP foci, ATP depletion after the
242 2DG treatment did not instantly trigger the formation of SG (Fig. S8). Consistent with recent
243 findings (Jain, Wheeler et al., 2016), the present results suggest that SG formation requires
244 ATP. We also noted that Hsp104-GFP foci and SG did not co-localize, indicating that these
245 structures are derived from distinct mechanisms (Fig. S8). Therefore, the artificial depletion
246 of ATP may trigger abnormal protein aggregation in living yeast cells.

247

248 ATP homeostasis is required for the protection of cells from cytotoxicity caused by
249 protein aggregation

250 Protein aggregation is often associated with neurodegenerative diseases, such as Alzheimer's,
251 Huntington's, and Parkinson's diseases (Eftekharzadeh, Hyman et al., 2016). Mitochondrial
252 failure has also been associated with many neurodegenerative diseases; however, it currently
253 remains unclear whether energy failure causes protein aggregation because mitochondria also
254 produce cytotoxic reactive oxygen species (ROS). (Bhat, Dar et al., 2015, Pathak, Berthet et
255 al., 2013). The abnormal aggregation of α-synuclein has been implicated in Parkinson's
256 disease (Lashuel, Overk et al., 2013). To clarify whether ATP prevents the formation of
257 cytotoxic protein aggregation, we examined the toxicity of α-synuclein-GFP (Syn-GFP) in
258 budding yeast. As reported previously, the expression of Syn-GFP exhibited negligible
259 toxicity against wild-type yeast when expressed under the inducible *GAL1* promotor (Fig. 5A)
260 (Outeiro & Lindquist, 2003, Sharma, Brandis et al., 2006, Wijayanti, Watanabe et al., 2015).
261 However, *snf1Δ*, *adk1Δ*, and *bas1Δ* were hypersensitive to the expression of Syn-GFP (Fig.
262 5A). We also found that *rpn4Δ*, which encodes a key transcription factor for proteasomal
263 subunits (Xie & Varshavsky, 2001), was very sensitive to Syn-GFP (Fig. 5A), which is
264 consistent with the concept that Syn-GFP is degraded in the ubiquitin-proteasomal pathway in
265 yeast (Tofaris, Kim et al., 2011, Wijayanti et al., 2015). We then visualized the cellular
266 localization of Syn-GFP. Consistent with previous findings (Willingham, Outeiro et al., 2003),
267 Syn-GFP expressed in yeast mainly localized to the plasma membrane (Fig. 5B, C). In
268 addition to the plasma membrane, we found that Syn-GFP localized to punctate structures,
269 most likely corresponding to protein aggregation (Fig. 5B, C). Punctate structures were not as
270 obvious in *rpn4Δ* cells defective in proteasomes, suggesting that the accumulation of
271 Syn-GFP puncta was not simply due to defective degradation.
272

273 To investigate whether a high level of ATP protects cells from toxic protein aggregation, we
274 added extra adenine to the medium (Fig. 5D). A previous study demonstrated that the addition
275 of 300 μM adenine to the medium increased ATP levels from 4 to 5.5 mM in wild-type cells
276 and from 1 to 4 mM in *bas1Δ* cells (Gauthier et al., 2008) (similar results are shown in Fig.
277 1E), but induced negligible or no changes in *adk1Δ* cells (from 2 to 2 mM) (Gauthier et al.,
278 2008). Consistent with our hypothesis, the addition of adenine reduced Syn-GFP toxicity and
279 aggregation in *bas1Δ*, but not *adk1Δ* cells (Fig. 5D). Thus, a high level of ATP prevented
280 Syn-GFP aggregation and toxicity.
281

282 We examined another model protein involved in neurodegenerative diseases. PolyQ
283 containing the huntingtin protein is susceptible to aggregation and has been implicated in
284 Huntington's disease (Jiang, Poirier et al., 2005). We investigated the toxicity of Htt103Q, a
285 mutant form of the huntingtin protein that is also susceptible to aggregation and causes
286 cytotoxicity in yeast (Meriin, Zhang et al., 2002). Consistent with the concept that a high level
287 of ATP prevents protein aggregation, the ATP homeostasis mutants *snf1Δ*, *adk1Δ*, *snf1Δ*
288 *adk1Δ*, and *bas1Δ* were very sensitive to Htt103Q expression (Fig. S9).
289
290 Proteasomes are essential for the removal of protein aggregates induced by ATP
291 depletion
292 Protein aggregation caused by ATP depletion was cytotoxic (Figs. 3B and 5A) and was not
293 easily dissolved after ATP repletion (Fig. 4). To identify a pathway that is essential for the
294 removal of aggregates, we examined the involvement of proteasomes and autophagy.
295
296 The deletion of *RPN4*, which encodes a transcription factor of proteasomal genes (Xie &
297 Varshavsky, 2001), down-regulated proteasomal activity (Kruegel, Robison et al., 2011) and
298 resulted in synthetic growth defects with *adk1Δ*, *snf1Δ*, *bas1Δ* at a high temperature of 38°C
299 and in the presence of H_2O_2 (Fig. 5E). In contrast to proteasomes, autophagy did not appear to
300 have genetic interactions with the above mutants (Fig. 5E). The deletion of an essential
301 component of the autophagic pathway, *ATG1* did not affect the sensitivity of *adk1Δ*, *snf1Δ*,
302 *bas1Δ* to a high temperature of 38°C or to H_2O_2 (Fig. 5E). We also did not observe the
303 accumulation of Hsp104-GFP foci in the autophagy mutants *atg1Δ*, *atg8Δ*, and *atg13Δ* (not
304 shown).
305
306 To investigate the involvement of proteasomes in the removal of protein aggregates after the
307 transient depletion of ATP, we pretreated cells with the proteasomal inhibitor MG132 or
308 DMSO and examined the kinetics for the formation of Hsp104-GFP foci after the 2DG
309 treatment (Fig. 5F) using the drug-sensitive yeast strain Y13206 (Piotrowski, Li et al., 2017).
310 Under both conditions, more than 90% of cells exhibited Hsp104-GFP foci within 30 min of
311 the 2DG treatment. More than two-thirds of Hsp104-GFP foci dissolved in the DMSO control,
312 while less than one-third dissolved in MG132-treated samples, indicating that proteasomes
313 are required for the dissolution process (Fig. 5F).

314 **DISCUSSION**

315 In the present study, we demonstrated for the first time that the Snf1 complex, budding yeast
316 AMPK, is required for the stable maintenance of cellular ATP levels (ATP homeostasis) in
317 collaboration with Adk1 (Fig. 6A). This function of the Snf1 complex in ATP homeostasis is
318 independent of glucose levels in the medium and Mig1, the major transcriptional repressor
319 involved in glucose repression (Fig. S1); therefore, this is distinct from its well-characterized
320 role in adaptation to glucose limitations. The activity of the Snf1 kinase complex may be
321 sharply tuned depending on the intracellular levels of adenine nucleotides or other metabolites
322 indicative of cellular energy to prevent a rapid ATP catastrophe (Fig. 2), even in the presence
323 of sufficient amounts of glucose. It is important to note that the reductions observed in
324 intracellular ATP levels in *snf1Δ* cells in the presence of glucose were overlooked in previous
325 biochemical analyses, again demonstrating the usefulness of QUEEN-based ATP imaging.
326
327 Since the deletion of *BAS1* induced the greatest reduction in ATP levels and is epistatic to
328 *snf1Δ*, a large pool size of adenine nucleotides is a prerequisite for ATP homeostasis. This
329 assumption is reasonable because the pool size of recyclable ATP restricts ATP levels based
330 on the rapid turnover rate of ATP. Bas1 maintains the pool size of ATP by balancing ATP
331 synthesis and irreversible decreases, such as incorporation into RNA and DNA (following
332 conversion to deoxy-ATP), degradation, and excretion in rapidly proliferating yeasts.
333
334 The decreases observed in ATP levels in the ATP mutant cells were confirmed by our
335 biochemical measurements (Figs. 1 and S3). The biochemical assay also revealed that ADP
336 levels decreased in ATP mutants, similar to ATP levels, and, as a consequence, ATP/ADP
337 ratios, indicators of cellular energy charges, remained largely unchanged. On the other hand,
338 the sum of ATP and ADP levels, indicators of the pool size of adenine nucleotides, decreased
339 in the mutants, which may explain the instability observed in ATP levels. While cytosolic
340 ATP levels were reduced and unstable in *snf1Δadk1Δ* cells, high levels of ATP may
341 accumulate in intracellular membrane compartments (*e.g.*, vacuoles, lysosomes, and
342 mitochondria) that were not visualized by the QUEEN, which would increase the average
343 ATP level of whole cells (Fig. 1B, C).
344
345 We also showed that key regulators of ATP homeostasis play roles in preventing cytotoxic
346 protein aggregation in budding yeast (Fig. 6B). The common feature associated with these
347 mutants is reduced ATP levels, suggesting that high ATP levels are essential for protein
348 solubilization.

349

350 A proteomic study suggested that the main role of ATP changes depending on its level. At
351 levels lower than 0.5 mM, ATP mainly serves as a substrate for enzymes, such as protein
352 kinases and heat shock protein chaperones, whereas at levels higher than 2 mM, ATP may
353 exert solubilizing effects on disordered proteins (Sridharan et al., 2019). ATP homeostasis
354 may also be required to constantly drive proteasomal protein degradation, which requires high
355 levels of ATP (Benaroudj, Zwickl et al., 2003, Tanaka, Waxman et al., 1983).
356

357 Previous biochemical measurements indicated that although ATP levels were lower in *adk1*
358 and *bas1* mutants than in the wild type, these mutants still had ATP levels that were higher
359 than 2 mM (Gauthier et al., 2008). This does not directly explain the accumulation of protein
360 aggregates in these mutants (Fig. 3) because most proteins are expected to be soluble at > 2
361 mM ATP (Sridharan et al., 2019). In this study, we explained this discrepancy by using the
362 biosensor-based ATP imaging technique we developed (Takaine et al., 2019, Yaginuma et al.,
363 2014). The visualization of ATP dynamics in living cells at the single cell level revealed that
364 ATP repeatedly undergoes transient depletion (the ATP catastrophe) in AMPK and ADK
365 mutants, which explains how aggregation-prone proteins aggregate and cause cytotoxicity. A
366 similar, but distinct, instability in ATP was observed in *bas1Δ*, further confirming that the
367 ATP catastrophe causes protein aggregation. Although severe ATP depletion in these mutants
368 was gradually recovered by as yet uncharacterized negative feedback regulation, the duration
369 period of ~15 min with reduced ATP levels may induce some proteins to form aggregates that
370 last for generations.
371

372 A recent study revealed that forced energy (ATP) depletion from budding yeast cells induced
373 extensive cytoplasmic reorganization, including increases in macromolecular (ribosome)
374 crowding, the emergence of numerous membrane-less organelles, and the polymerization of
375 eukaryotic translation initiation factor 2B (Marini et al., 2020). Another recent study showed
376 that the depletion of ATP triggered the "viscoadaptation" of yeast cytoplasm by an as yet
377 unknown mechanism, and induced increases in viscosity and decreases in biomolecular
378 solubility, thereby enhancing phase separation (Persson et al., 2020). These findings imply
379 that malfunctional ATP homeostasis may induce undesirable and dysregulated biomolecular
380 assemblies driven by enhanced liquid-liquid phase separation and molecular crowding. The
381 present study using ATP mutant cells is the first to demonstrate the consequence of failed
382 ATP homeostasis under physiologically relevant conditions and highlights the biological
383 significance of ATP homeostasis.

384

385 Many neurodegenerative diseases, such as Alzheimer's, Huntington's, and Parkinson's
386 diseases, are associated with protein aggregation (Eisele, Monteiro et al., 2015, Josefson et al.,
387 2017). On the other hand, based on a large body of evidence, mitochondrial dysfunction and
388 accompanying energy failure in nerve cells may result in many types of neurodegenerative
389 diseases (Haelterman, Yoon et al., 2014, Pathak et al., 2013). Previous studies demonstrated
390 that ATP levels in the brain were decreased in patients with early Parkinson's disease (Mochel,
391 N'Guyen et al., 2012) and also that ATP synthesis in the brain was not properly regulated in
392 patients with early Huntington's disease (Hattingen, Magerkurth et al., 2009) and in the
393 corresponding mouse model (Mochel, Durant et al., 2012). Therefore, protein aggregation
394 induced by the ATP catastrophe, as revealed in the present study, may link energy failure and
395 protein aggregation, providing a comprehensive insight into the onset of neurodegenerative
396 diseases. Further studies are warranted to clarify whether the ATP catastrophe also occurs in
397 the neurons of patients at risk of neurodegenerative diseases or in the elderly. However,
398 neither biochemical measurements nor mass spectrometry is capable of detecting the ATP
399 catastrophe because of their insufficient time and space resolution. Therefore, an ATP
400 imaging approach using the yeast system will be the leading model for elucidating the
401 molecular mechanisms underlying ATP homeostasis and ATP catastrophe-induced protein
402 aggregation.
403

404 A recent study reported that the activation of AMPK by metformin ameliorated the
405 progression of Huntington's disease in a mouse model (Arnoux, Willam et al., 2018), and the
406 potential therapeutic use of metformin for neurodegenerative diseases is being discussed
407 (Rotermund, Machetanz et al., 2018). Furthermore, the involvement of ATP and ADK in
408 preventing the manifestation of Parkinson's disease in mouse models and patients has been
409 proposed (Garcia-Esparcia, Hernandez-Ortega et al., 2015, Nakano, Imamura et al., 2017).
410 Protein aggregation induced by the ATP catastrophe may be a general mechanism for the
411 development of proteinopathies. The present study using ATP imaging revealed a
412 physiological consequence of a failure in ATP homeostasis in living cells for the first time
413 and suggests that ATP homeostasis has potential as a target for preventing/treating
414 neurodegenerative diseases.

415 **MATERIALS AND METHODS**

416 Yeast strains and plasmids

417 The budding yeast strains and plasmids used in the present study are listed in Supplementary
418 Tables S1 and S2, respectively. These strains were constructed by a PCR-based method
419 (Janke, Magiera et al., 2004) and genetic crosses. The yeast knockout strain collection was
420 originally purchased from GE Healthcare (cat. # YSC1053).
421

422 Media and cell culture

423 The standard technique for the yeast culture and manipulation was used (Guthrie & Fink,
424 2002). Synthetic medium (SC) was prepared as described by Hanscho et al. (Hanscho,
425 Ruckerbauer et al., 2012). 2-Deoxy-D-glucose (2DG), tunicamycin, and MG132 were
426 purchased from FUJIFILM Wako (cat. # 046-06483, 202-08241, and 139-18451,
427 respectively). Tunicamycin and MG132 were dissolved in dimethylsulfoxide (DMSO) to
428 make stock solutions (5 mg/ml and 42 mM, respectively). Cells were grown to the mid-log
429 phase at 30°C in SC before imaging unless otherwise noted.
430

431 Microscopy

432 Cells expressing Hsp104-GFP or GFP-Ubc9ts were concentrated by centrifugation and
433 sandwiched between a slide and coverslip (No. 1.5 thickness, Matsunami, Osaka, Japan).
434 Immobilized cells were imaged using an inverted fluorescent microscope (Eclipse Ti-E,
435 Nikon) equipped with an Apo TIRF 100× Oil DIC N2/NA 1.49 objective lens and
436 electron-multiplying charge-coupled device camera (iXon3 DU897E-CS0-#BV80, Andor) at
437 approximately 25°C. The Hsp104-GFP and GFP-Ubc9ts fluorescent signal was collected
438 from stacks of 11 *z*-sections spaced by 0.5 μm, and the maximum projections of the optical
439 sections were shown in Figs. 4, 5, and S6. Cells expressing QUEEN were immobilized on a
440 concanavalin A-coated 35-mm glass-bottomed dish (#3971-035, No. 1.5 thickness, IWAKI).
441 The dish was filled with an excess amount of medium (4.5–5 ml) against the cell volume to
442 minimize changes in the chemical compositions of the medium during observations. QUEEN
443 fluorescence was acquired as previously described (Takaine et al., 2019). Cells expressing
444 Syn-GFP were immobilized on a slide glass as described above, and the fluorescence signal
445 was collected from a single *z*-plane using an inverted fluorescent microscope (Eclipse Ti2-E,
446 Nikon, Tokyo, Japan) equipped with a CFI Plan Apoλ100× Oil DIC/NA1.45 objective lens

447 and CMOS image sensor (DS-Qi2, Nikon). Images of cells were acquired from several fields
448 of view for each experimental condition.
449

450 ## Biochemical measurements of ATP and ADP

451 Whole cell extracts were prepared according to Seo et al. (Seo, Lau et al., 2017) with slight
452 modifications. Mid-log cells were harvested in a 1.6-ml microtube by centrifugation and
453 resuspended in 1 ml fresh SC or 40 mM 2DG medium (for ATP depletion). After a 10-min
454 incubation at 30°C, a small fraction of cells (50 µl) was removed for the measurement of cell
455 numbers and optical density, and the remaining cells were pelleted and resuspended in 0.75
456 ml of 90% acetone. The suspension was incubated at 90°C for 15 min to evaporate acetone.
457 The remaining solution (30–35 µl) was centrifuged at 20,000×*g* at 4°C for 3 min. The
458 supernatant was mixed with 450 µl of TE (10 mM Tris-HCl, pH 8.0, and 1 mM
459 ethylenediaminetetraacetic acid). These extracts were stored at -80°C until analyzed. ATP and
460 ADP levels were measured using the ATP determination kit (Invitrogen) and EnzyLight ADP
461 assay kit (EADP-100, Funakoshi), respectively, according to the manufacturers' instructions.
462 Luminescence was measured using an Enspire multimode plate reader (PerkinElmer). All
463 samples were assayed in duplicate. ATP and ADP levels were normalized for an optical
464 density at 600 nm of the initial cell suspension assessed by BioSpectrometer (Eppendorf).
465

466 ## Data analysis

467 Numerical data were plotted using KaleidaGraph software ver. 4.5.1 (Synergy Software) and
468 R studio software ver. 3.4.1 (R Core Team, 2017). Means, SDs, and *p* values were calculated
469 using Excel software (Microsoft, WA, US). Significance between two sets of data was tested
470 using the unpaired one-tailed Welch's *t*-test unless otherwise noted, and was indicated by an
471 asterisk or *p* value. Data were sometimes represented by a dot plot that shows distribution
472 characteristics in extensive detail. The horizontal bar in the dot plot indicates the average of
473 each population. All measurements were repeated at least twice to confirm reproducibility.
474 ATP levels in yeast cells were estimated using QUEEN-based ratiometric imaging,
475 as previously described (Takaine, 2019), (Takaine et al., 2019). The QUEEN ratio is
476 proportional to ATP levels and pseudo-colored to reflect its value throughout the present
477 study. The mean QUEEN ratio inside of a cell represents the intracellular ATP level of the
478 cell.
479 The autocorrelation functions (ACF) of oscillations in the QUEEN ratio were
480 calculated using R studio software. The apparent period of oscillation was estimated from the

positive second peak of the correlation coefficient, which was outside the 95% confidence interval and significant ($p < 0.05$), rejecting the assumption that there is no correlation.

ACKNOWLEDGMENTS

We are grateful to the Yeast Genetic Resource Center, Y. Ohya, K. Ohashi, H. Takagi, D. Watanabe, and J. Frydman for providing the yeast strains and plasmids. We thank the members of the Yoshida/Takaine laboratories for their support. This work was supported by JSPS grants 16H04781 (S.Y. and M.T.), 15K18525 (M.T.), and 19K06654 (M.T.) and the Takeda Science Foundation (S.Y.). This work was also supported by the joint research program of the Institute for Molecular and Cellular Regulation, Gunma University, Japan.

AUTHOR CONTRIBUTIONS

M.T. and S.Y. conceived and designed the project. M.T. conducted experiments and the data analysis. H.I. provided a key reagent and expertise. M.T. and S.Y wrote the manuscript with input from H.I.

CONFLICT OF INTEREST

The authors declare no competing interests.

499 **REFERENCES**

500 Arnoux I, Willam M, Griesche N, Krummeich J, Watari H, Offermann N, Weber S, Narayan Dey P, Chen C,
501 Monteiro O, Buettner S, Meyer K, Bano D, Radyushkin K, Langston R, Lambert JJ, Wanker E, Methner A,
502 Krauss S, Schweiger S et al. (2018) Metformin reverses early cortical network dysfunction and behavior changes
503 in Huntington's disease. *Elife* 7

504 Baryshnikova A (2016) Systematic Functional Annotation and Visualization of Biological Networks. *Cell*
505 *Syst* 2: 412-21

506 Benaroudj N, Zwickl P, Seemuller E, Baumeister W, Goldberg AL (2003) ATP hydrolysis by the proteasome
507 regulatory complex PAN serves multiple functions in protein degradation. *Mol Cell* 11: 69-78

508 Bhat AH, Dar KB, Anees S, Zargar MA, Masood A, Sofi MA, Ganie SA (2015) Oxidative stress,
509 mitochondrial dysfunction and neurodegenerative diseases; a mechanistic insight. *Biomed Pharmacother* 74:
510 101-10

511 Carlson M (1999) Glucose repression in yeast. *Curr Opin Microbiol* 2: 202-7

512 Cherry JM, Hong EL, Amundsen C, Balakrishnan R, Binkley G, Chan ET, Christie KR, Costanzo MC,
513 Dwight SS, Engel SR, Fisk DG, Hirschman JE, Hitz BC, Karra K, Krieger CJ, Miyasato SR, Nash RS, Park J,
514 Skrzypek MS, Simison M et al. (2012) Saccharomyces Genome Database: the genomics resource of budding
515 yeast. *Nucleic Acids Res* 40: D700-5

516 Daignan-Fornier B, Fink GR (1992) Coregulation of purine and histidine biosynthesis by the transcriptional
517 activators BAS1 and BAS2. *Proc Natl Acad Sci U S A* 89: 6746-50

518 Denis V, Boucherie H, Monribot C, Daignan-Fornier B (1998) Role of the myb-like protein bas1p in
519 Saccharomyces cerevisiae: a proteome analysis. *Mol Microbiol* 30: 557-66

520 Edelman AM, Blumenthal DK, Krebs EG (1987) Protein serine/threonine kinases. *Annu Rev Biochem* 56:
521 567-613

522 Eftekharzadeh B, Hyman BT, Wegmann S (2016) Structural studies on the mechanism of protein aggregation
523 in age related neurodegenerative diseases. *Mech Ageing Dev* 156: 1-13

524 Eisele YS, Monteiro C, Fearns C, Encalada SE, Wiseman RL, Powers ET, Kelly JW (2015) Targeting
525 protein aggregation for the treatment of degenerative diseases. *Nat Rev Drug Discov* 14: 759-80

526 Garcia-Esparcia P, Hernandez-Ortega K, Ansoleaga B, Carmona M, Ferrer I (2015) Purine metabolism gene
527 deregulation in Parkinson's disease. *Neuropathol Appl Neurobiol* 41: 926-40

528 Gauthier S, Coulpier F, Jourdren L, Merle M, Beck S, Konrad M, Daignan-Fornier B, Pinson B (2008)
529 Co-regulation of yeast purine and phosphate pathways in response to adenylic nucleotide variations. *Mol*
530 *Microbiol* 68: 1583-94

531 Ghillebert R, Swinnen E, Wen J, Vandesteene L, Ramon M, Norga K, Rolland F, Winderickx J (2011) The
532 AMPK/SNF1/SnRK1 fuel gauge and energy regulator: structure, function and regulation. *FEBS J* 278: 3978-90

533 Guthrie C, Fink GR (2002) *Guide to yeast genetics and molecular and cell Biology: Part C*. Gulf Professional

534 Publishing,
535 Haelterman NA, Yoon WH, Sandoval H, Jaiswal M, Shulman JM, Bellen HJ (2014) A Mitocentric View of
536 Parkinson's Disease. *Annual Review of Neuroscience* 37: 137-159
537 Hanscho M, Ruckerbauer DE, Chauhan N, Hofbauer HF, Krahulec S, Nidetzky B, Kohlwein SD, Zanghellini
538 J, Natter K (2012) Nutritional requirements of the BY series of Saccharomyces cerevisiae strains for optimum
539 growth. *FEMS Yeast Res* 12: 796-808
540 Hardie DG, Carling D, Carlson M (1998) The AMP-activated/SNF1 protein kinase subfamily: metabolic
541 sensors of the eukaryotic cell? *Annu Rev Biochem* 67: 821-55
542 Hardie DG, Schaffer BE, Brunet A (2016) AMPK: An Energy-Sensing Pathway with Multiple Inputs and
543 Outputs. *Trends Cell Biol* 26: 190-201
544 Hattingen E, Magerkurth J, Pilatus U, Mozer A, Seifried C, Steinmetz H, Zanella F, Hilker R (2009)
545 Phosphorus and proton magnetic resonance spectroscopy demonstrates mitochondrial dysfunction in early and
546 advanced Parkinson's disease. *Brain* 132: 3285-97
547 Hayes MH, Peuchen EH, Dovichi NJ, Weeks DL (2018) Dual roles for ATP in the regulation of phase
548 separated protein aggregates in Xenopus oocyte nucleoli. *Elife* 7: e35224
549 Hedbacker K, Carlson M (2008) SNF1/AMPK pathways in yeast. *Front Biosci* 13: 2408-20
550 Herzig S, Shaw RJ (2017) AMPK: guardian of metabolism and mitochondrial homeostasis. *Nature Reviews*
551 *Molecular Cell Biology* 19: 121
552 Hoyle NP, Castelli LM, Campbell SG, Holmes LE, Ashe MP (2007) Stress-dependent relocalization of
553 translationally primed mRNPs to cytoplasmic granules that are kinetically and spatially distinct from P-bodies. *J*
554 *Cell Biol* 179: 65-74
555 Jain S, Wheeler JR, Walters RW, Agrawal A, Barsic A, Parker R (2016) ATPase-Modulated Stress Granules
556 Contain a Diverse Proteome and Substructure. *Cell* 164: 487-98
557 Janke C, Magiera MM, Rathfelder N, Taxis C, Reber S, Maekawa H, Moreno-Borchart A, Doenges G,
558 Schwob E, Schiebel E, Knop M (2004) A versatile toolbox for PCR-based tagging of yeast genes: new
559 fluorescent proteins, more markers and promoter substitution cassettes. *Yeast* 21: 947-62
560 Janssen E, Dzeja PP, Oerlemans F, Simonetti AW, Heerschap A, de Haan A, Rush PS, Terjung RR, Wieringa
561 B, Terzic A (2000) Adenylate kinase 1 gene deletion disrupts muscle energetic economy despite metabolic
562 rearrangement. *EMBO J* 19: 6371-81
563 Jiang H, Poirier MA, Ross CA (2005) A structure-based analysis of huntingtin mutant polyglutamine
564 aggregation and toxicity: evidence for a compact beta-sheet structure. *Human Molecular Genetics* 14: 765-774
565 Josefson R, Andersson R, Nyström T (2017) How and why do toxic conformers of aberrant proteins
566 accumulate during ageing? *Essays In Biochemistry* 61: 317
567 Kaganovich D, Kopito R, Frydman J (2008) Misfolded proteins partition between two distinct quality control
568 compartments. *Nature* 454: 1088-95

569 Kruegel U, Robison B, Dange T, Kahlert G, Delaney JR, Kotireddy S, Tsuchiya M, Tsuchiyama S,
570 Murakami CJ, Schleit J, Sutphin G, Carr D, Tar K, Dittmar G, Kaeberlein M, Kennedy BK, Schmidt M (2011)
571 Elevated proteasome capacity extends replicative lifespan in Saccharomyces cerevisiae. *PLoS Genet* 7:
572 e1002253
573 Lashuel HA, Overk CR, Oueslati A, Masliah E (2013) The many faces of alpha-synuclein: from structure and
574 toxicity to therapeutic target. *Nat Rev Neurosci* 14: 38-48
575 Ljungdahl PO, Daignan-Fornier B (2012) Regulation of amino acid, nucleotide, and phosphate metabolism in
576 Saccharomyces cerevisiae. *Genetics* 190: 885-929
577 Marini G, Nuske E, Leng W, Alberti S, Pigino G (2020) Reorganization of budding yeast cytoplasm upon
578 energy depletion. *Mol Biol Cell* 31: 1232-1245
579 Meriin AB, Zhang X, He X, Newnam GP, Chernoff YO, Sherman MY (2002) Huntington toxicity in yeast
580 model depends on polyglutamine aggregation mediated by a prion-like protein Rnq1. *J Cell Biol* 157: 997-1004
581 Mochel F, Durant B, Meng X, O'Callaghan J, Yu H, Brouillet E, Wheeler VC, Humbert S, Schiffmann R,
582 Durr A (2012) Early alterations of brain cellular energy homeostasis in Huntington disease models. *J Biol Chem*
583 287: 1361-70
584 Mochel F, N'Guyen TM, Deelchand D, Rinaldi D, Valabregue R, Wary C, Carlier PG, Durr A, Henry PG
585 (2012) Abnormal response to cortical activation in early stages of Huntington disease. *Mov Disord* 27: 907-10
586 Nakano M, Imamura H, Sasaoka N, Yamamoto M, Uemura N, Shudo T, Fuchigami T, Takahashi R,
587 Kakizuka A (2017) ATP Maintenance via Two Types of ATP Regulators Mitigates Pathological Phenotypes in
588 Mouse Models of Parkinson's Disease. *EBioMedicine* 22: 225-241
589 Outeiro TF, Lindquist S (2003) Yeast cells provide insight into alpha-synuclein biology and pathobiology.
590 *Science* 302: 1772-5
591 Patel A, Malinovska L, Saha S, Wang J, Alberti S, Krishnan Y, Hyman AA (2017) ATP as a biological
592 hydrotrope. *Science* 356: 753-756
593 Pathak D, Berthet A, Nakamura K (2013) Energy failure: does it contribute to neurodegeneration? *Ann*
594 *Neurol* 74: 506-16
595 Persson LB, Ambati VS, Brandman O (2020) Cellular Control of Viscosity Counters Changes in
596 Temperature and Energy Availability. *Cell*
597 Piotrowski JS, Li SC, Deshpande R, Simpkins SW, Nelson J, Yashiroda Y, Barber JM, Safizadeh H, Wilson
598 E, Okada H, Gebre AA, Kubo K, Torres NP, LeBlanc MA, Andrusiak K, Okamoto R, Yoshimura M,
599 DeRango-Adem E, van Leeuwen J, Shirahige K et al. (2017) Functional annotation of chemical libraries across
600 diverse biological processes. *Nature Chemical Biology* 13: 982
601 Pu Y, Li Y, Jin X, Tian T, Ma Q, Zhao Z, Lin SY, Chen Z, Li B, Yao G, Leake MC, Lo CJ, Bai F (2019)
602 ATP-Dependent Dynamic Protein Aggregation Regulates Bacterial Dormancy Depth Critical for Antibiotic
603 Tolerance. *Mol Cell* 73: 143-156 e4

604 R Core Team (2017) R: A Language and Environment for Statistical Computing. In Vienna, Austria: R
605 Foundation for Statistical Computing
606 Rotermund C, Machetanz G, Fitzgerald JC (2018) The Therapeutic Potential of Metformin in
607 Neurodegenerative Diseases. *Front Endocrinol (Lausanne)* 9: 400
608 Seo AY, Lau P-W, Feliciano D, Sengupta P, Gros MAL, Cinquin B, Larabell CA, Lippincott-Schwartz J
609 (2017) AMPK and vacuole-associated Atg14p orchestrate μ-lipophagy for energy production and long-term
610 survival under glucose starvation. *eLife* 6: e21690
611 Sharma N, Brandis KA, Herrera SK, Johnson BE, Vaidya T, Shrestha R, DebBurman SK (2006) α-synuclein
612 budding yeast model. *Journal of Molecular Neuroscience* 28: 161-178
613 Sridharan S, Kurzawa N, Werner T, Gunthner I, Helm D, Huber W, Bantscheff M, Savitski MM (2019)
614 Proteome-wide solubility and thermal stability profiling reveals distinct regulatory roles for ATP. *Nat Commun*
615 10: 1155
616 Takaine M (2019) QUEEN-based Spatiotemporal ATP Imaging in Budding and Fission Yeast. *Bio-Protocol*
617 9: e3320
618 Takaine M, Ueno M, Kitamura K, Imamura H, Yoshida S (2019) Reliable imaging of ATP in living budding
619 and fission yeast. *J Cell Sci* 132
620 Tanaka K, Waxman L, Goldberg AL (1983) ATP serves two distinct roles in protein degradation in
621 reticulocytes, one requiring and one independent of ubiquitin. *J Cell Biol* 96: 1580-5
622 Tofaris GK, Kim HT, Hourez R, Jung JW, Kim KP, Goldberg AL (2011) Ubiquitin ligase Nedd4 promotes
623 alpha-synuclein degradation by the endosomal-lysosomal pathway. *Proc Natl Acad Sci U S A* 108: 17004-9
624 Usaj M, Tan Y, Wang W, VanderSluis B, Zou A, Myers CL, Costanzo M, Andrews B, Boone C (2017)
625 TheCellMap.org: A Web-Accessible Database for Visualizing and Mining the Global Yeast Genetic Interaction
626 Network. *G3 (Bethesda)* 7: 1539-1549
627 Wijayanti I, Watanabe D, Oshiro S, Takagi H (2015) Isolation and functional analysis of yeast ubiquitin
628 ligase Rsp5 variants that alleviate the toxicity of human α-synuclein. *The Journal of Biochemistry* 157: 251-260
629 Willingham S, Outeiro TF, DeVit MJ, Lindquist SL, Muchowski PJ (2003) Yeast genes that enhance the
630 toxicity of a mutant huntingtin fragment or alpha-synuclein. *Science* 302: 1769-72
631 Wilson WA, Hawley SA, Hardie DG (1996) Glucose repression/derepression in budding yeast: SNF1 protein
632 kinase is activated by phosphorylation under derepressing conditions, and this correlates with a high AMP:ATP
633 ratio. *Curr Biol* 6: 1426-34
634 Xiao B, Heath R, Saiu P, Leiper FC, Leone P, Jing C, Walker PA, Haire L, Eccleston JF, Davis CT, Martin
635 SR, Carling D, Gamblin SJ (2007) Structural basis for AMP binding to mammalian AMP-activated protein
636 kinase. *Nature* 449: 496-500
637 Xie Y, Varshavsky A (2001) RPN4 is a ligand, substrate, and transcriptional regulator of the 26S
638 proteasome: a negative feedback circuit. *Proc Natl Acad Sci U S A* 98: 3056-61

639 Yaginuma H, Kawai S, Tabata KV, Tomiyama K, Kakizuka A, Komatsuzaki T, Noji H, Imamura H (2014)
640 Diversity in ATP concentrations in a single bacterial cell population revealed by quantitative single-cell imaging.
641 *Sci Rep* 4: 6522
642

643 **FIGURE LEGENDS**

644 Fig. 1 Interconversion and active synthesis of adenine nucleotides are important for
645 ATP homeostasis

646 (A) Adk1 and Snf1 synergistically control cellular ATP levels. QUEEN ratio images of ATP
647 homeostasis mutant cells grown in medium containing 2% glucose. The asterisk indicates an
648 example of cells with significantly reduced ATP levels. (B) The mean QUEEN ratios of cells
649 were translated to ATP levels and shown in a dot plot. The horizontal bar indicates the mean
650 of each population. Asterisks indicate *p* values versus WT: *=1.5×10^{-59}, **=2.3×10^{-34},
651 ***=2.9×10^{-117}. CV: coefficient of variance. N = 134–276 cells were scored.
652 (C) Biochemical measurements of cellular ATP levels. ATP levels in cells of the indicated
653 genotypes were measured as described in the Materials and Methods. Data are the mean ±
654 1SD (error bars) (N = 4). An asterisk indicates a *p* value of 0.03 versus WT. (D) QUEEN ratio
655 images of *bas1Δ* cells grown in 2% glucose medium. Growth in media supplemented with
656 0.11 mg/ml adenine partially restored the low ATP phenotype of *bas1*Δ. (E) ATP levels in
657 cells shown in *D* were plotted. Asterisks indicate *p* values: *=2.3×10^{-160}, **=8.8×10^{-12} (versus
658 WT in glucose), ***=3.6×10^{-20} (versus *bas1*Δ in glucose). CV: coefficient of variance. N =
659 186–296 cells were scored. (F) ATP levels in WT and *bas1Δ* cells were measured as
660 described in *C*. Data are the mean ± 1SD (error bars) (N = 4). An asterisk indicates a *p* value
661 of 8.5×10^{-5} versus WT.

662

663 Fig. 2 Temporal fluctuations in ATP levels in *snf1*Δ*adk1*Δ and *bas1*Δ cells

664 (A, C) Time-lapse imaging of QUEEN in *snf1*Δ *adk1*Δ cells in 2% glucose medium. Images
665 at the representative time points were shown. The QUEEN ratio decreased twice (indicated by
666 arrowheads) within a short interval. See also Movie S1. Data were converted into ATP levels
667 and plotted in (C). (B, D) Another example of the time-lapse imaging of QUEEN in
668 *snf1*Δ*adk1*Δ cells in 2% glucose medium. The QUEEN ratio decreased twice (indicated by
669 arrowheads) with a long interval. See also Movie S2. Data were converted into ATP levels
670 and plotted in (D). (E) Time-lapse imaging of QUEEN in *bas1*Δ in 2% glucose medium. ATP
671 levels in the mother (cell-1) and daughter (cell-2) were plotted at the bottom. Images at the
672 representative time points were shown on the top. Note that the QUEEN ratio is synchronized
673 until cells undergo separation at the time point of 76 min indicated by an arrow. After
674 separation, each cell has a unique periodic cycle of ATP. The movie is available in Movie S3.
675 White scale bar = 5 μm.

676

677 Fig. 3 ATP homeostasis is required to prevent protein aggregation
678 (A) Functional landscape of known interactors of ATP mutants. Negative genetic interactors
679 of the indicated gene were derived from the SGD database (https://www.yeastgenome.org/)
680 (Cherry, Hong et al., 2012) and overlaid on a functional map based on the global genetic
681 interaction network of the yeast genome (Baryshnikova, 2016, Usaj et al., 2017). *URA6*
682 encodes an uridylate kinase that is essential for viability, which also exhibits adenylate kinase
683 activity. (B) Each strain of the indicated genotype was serially diluted (five-fold), spotted on
684 SC + 2% glucose medium, and grown under the indicated stress conditions. Photos were
685 taken after 2-3 days. (C) Formation of Hsp104-GFP foci in ATP homeostasis mutants. The
686 GFP signal (inverted grayscale) was imaged in the log phase culture of the indicated mutant
687 cells expressing Hsp104-GFP at 35°C. (D) Quantification of data shown in (C). Data from
688 similar experiments using strains expressing Pab1-GFP, instead of Hsp104-GFP, were also
689 plotted. Values are the mean ± 1SD (error bars). Asterisks indicate a significant difference
690 from WT ($p < 0.05$) (N=3–4). White scale bar = 5 μm.
691
692 Fig. 4 ATP depletion triggers protein aggregation in living yeast cells
693 (A) The formation of Hsp104-GFP foci after ATP depletion. Wild-type cells expressing
694 Hsp104-GFP were grown to the log phase at 35°C in medium containing 2% glucose. At the
695 time point of 0 min, medium was replaced with 20 mM 2DG (red) or 2% glucose (as a
696 control; blue). Cells were released back to media containing 2% glucose at the time point of
697 50 min. Cells were imaged at the indicated time points, classified, and scored according to the
698 number of Hsp104-GFP foci. Values are the mean (N = 3). Asterisks indicate a significant
699 difference from the 2% glucose treatment ($p < 0.05$). (B) Representative images of cells
700 analyzed in (A). (C) Formation of Ubc9-ts foci after ATP depletion. Cells expressing
701 GFP-Ubc9-ts under an inducible *GAL* promoter were grown in medium containing 2%
702 galactose (SC-gal) at 33°C, and medium was then exchanged with 2DG or SC-gal. After 30
703 min, cells were imaged and scored for the number of GFP-Ubc9-ts foci. Representative
704 images (inverted grayscale) are shown on the left and summarized on the right. Values are the
705 mean ± 1SD (error bars) (N = 4). White scale bar = 5 μm.
706
707 Fig. 5 Aggregation and cytotoxicity of α-synuclein depends on ATP homeostasis
708 (A) Each strain of the indicated genotype was transformed with an expression vector carrying
709 α-synuclein-GFP or GFP, serially diluted (five-fold), spotted on SC + 2% galactose plates,
710 and then grown at 30°C for 3 days. (B) The localization of α-synuclein-GFP in ATP mutants.
711 Cells were grown on galactose plates at 30°C for more than 42 h and then imaged.

712 Representative images of α-synuclein-GFP (inverted grayscale) are shown. (C) Quantification
713 of the data shown in (B). Cells were classified and scored for the localization pattern of
714 α-synuclein-GFP. The percentage of cells showing α-synuclein-GFP foci are plotted. Data are
715 the mean ± 1SD (error bars) from 3–6 independent observations. N = 33–380 cells were
716 scored in each measurement. *P* values versus WT are shown. N.S., no significance (p value >
717 0.05). (D) *(top)* Each strain of the indicated genotype was transformed with an expression
718 vector carrying α-synuclein-GFP and grown on galactose plates containing 0 mM (−
719 Adenine) or 0.3 mM (+ Adenine) adenine at 30°C for 3 days. *(bottom)* Cells were grown on
720 galactose plates in the absence or presence of adenine at 30°C for 41-45 h and then imaged.
721 The percentage of cells showing α-synuclein-GFP foci was plotted. Data are the mean ± 1SD
722 (error bars) from 5 independent transformants. N = 53–258 cells were scored in each
723 measurement. *P* values versus "– Adenine" are shown. (E) Each strain of the indicated
724 genotype was serially diluted (five-fold), spotted on SC + 2% glucose medium, and grown
725 under the indicated stress conditions. (F) Cells of the drug-sensitive strain Y13206 were
726 grown to the log phase at 37°C in medium containing 2% glucose and supplemented with
727 0.1% DMSO or 0.1% DMSO plus 42 μM MG132 at $t = -30$ min. At $t = 0$ min, these cells
728 were washed and released in medium containing 20 mM 2DG ± MG132, and cells were then
729 washed and released again in medium containing 2% glucose ± MG132. Cells were imaged at
730 the indicated time points and scored for the number of Hsp104-GFP foci. Data are the mean ±
731 1SD (error bars). Asterisks indicate a significant difference from DMSO ($p < 0.02$) (N=3).
732
733 Fig. 6 Models for ATP homeostasis and its role in proteostasis
734 (A) Schematic summary of the roles of Snf1, Adk1, and Bas1 in ATP homeostasis. (B) A
735 schematic model for ATP homeostasis preventing cytotoxic protein aggregation.

736 **SUPPLEMENTARY INFORMATION**

737 Supplementary figure legends

738 Fig. S1 AMPK is involved in the maintenance of cellular ATP levels in non-starving
739 cells

740 (A) Visualization of intracellular ATP levels in wild-type (WT) and *snf1Δ* cells using the
741 ATP sensor QUEEN. Cells were grown to the mid-log phase in SC-H medium containing the
742 indicated levels of glucose and then imaged. White scale bar = 5 μm. (B) *snf1Δ* cells had
743 lower ATP levels than wild-type cells. The mean QUEEN ratio inside a single cell (mean
744 QUEEN ratio/cell), which represents the intracellular ATP level of the cell, was quantified for
745 each cell from the ratio image. Data are the mean of the cell population ± 1SD (error bar)
746 normalized to wild-type cells. N = 105–193 cells were scored. Asterisks indicate a significant
747 difference from WT ($p < 0.05$). (C) *mig1Δ* cells had slightly lower ATP levels than wild-type
748 cells. Data are the mean of the cell population ± 1SD (error bar) normalized to wild-type cells.
749 N = 190–231 cells were scored. Asterisks indicate a significant difference between the two
750 strains.

751

752 Fig. S2 Adenylate kinase Adk1 is involved in the maintenance of cellular ATP levels

753 (A) QUEEN ratio images of wild-type and *adk1Δ* cells grown in 2% glucose or 2% galactose.
754 White scale bar = 5 μm. (B) Quantification of data shown in (A). The mean QUEEN ratio/cell
755 was quantified for each cell from ratio images. Values are the mean of the cell population ±
756 1SD (error bar). N = 182–236 cells were scored. Asterisks indicate a significant difference
757 from WT ($p < 0.05$).

758

759 Fig. S3 Biochemical measurements of ATP and ADP

760 (A) Biochemical measurements of cellular ADP levels. ADP levels in cells of the indicated
761 genotypes were measured as described in the Materials and Methods. Data are the mean ±
762 1SD (error bars) (N = 4). Asterisks indicate *p* values versus WT: *=6.0×10^{-4}, **=1.5×10^{-4}.
763 (B) 2DG depletes cellular ATP. ATP levels in WT cells incubated with medium containing
764 2% glucose or 40 mM 2DG for 10 min were biochemically measured. Relative ATP levels
765 were expressed as the ratios of ATP levels in glucose-treated cells. Data are the mean ± 1SD
766 (error bars) (N = 4). (C) ATP/ADP ratios in WT and ATP mutant cells. ATP/ADP ratios were
767 calculated from ATP and ADP levels measured using biochemical assays. Data are the mean
768 ± 1SD (error bars) (N = 4). An asterisk indicates a *p* value of 6.0×10^{-4} versus WT. (D) The
769 sums of ATP and ADP levels in WT and ATP mutant cells were calculated from ATP and
770 ADP levels measured using biochemical assays. Data are the mean ± 1SD (error bars) (N = 4).

771 Asterisks indicate *p* values versus WT: *=1.6×10^{-2}, **=1.0×10^{-4}.
772
773 Fig. S4 ATP levels in *bas1*Δ *snf1*Δ cells
774 (A) QUEEN ratio images of wild-type, *bas1Δ*, *snf1Δ*, and *bas1Δ snf1Δ* cells. (B)
775 Quantification of data shown in (A). The mean QUEEN ratio/cell was quantified for each cell
776 from ratio images. Data are shown as a dot plot. The horizontal bar in the plot indicates the
777 mean of each population. Significance between two sets of data was tested using the unpaired
778 two-tailed Welch's *t*-test and indicated by *p* values. N.S., no significance (*p*-value > 0.05).
779
780 Fig. S5 Time-lapse imaging of QUEEN in *snf1*Δ *adk1*Δ cells
781 Time-lapse imaging of QUEEN in *snf1*Δ *adk1*Δ cells in 2% glucose medium. An example of
782 a *snf1*Δ *adk1*Δ cell showing an irreversible decrease in the QUEEN ratio (indicated by an
783 arrowhead). In this case, the cell eventually died (indicated by an arrow). Images at the
784 representative time points were shown. The ATP level was plotted at the bottom. White scale
785 bar = 5 μm.
786
787 Fig. S6. Oscillatory behavior of the ATP level visualized in *bas1*Δ cells
788 (A) Another example of *bas1Δ* cells showing an oscillating QUEEN ratio. In this case,
789 cytokinesis had just been completed at t = 0 min. ATP levels in cell-1 and cell-2 were plotted
790 at the bottom. See also Movie S4. White scale bar = 5 μm. (B) Autocorrelation function of the
791 QUEEN ratio calculated from the data on cell-1 in Fig. 3E. Blue dotted lines indicate the 95%
792 confidence interval. An arrow indicates the second peak of the correlation and corresponds to
793 the apparent period.
794
795 Fig. S7 *In silico* analysis of interactors of ATP mutants
796 Genetic and physical interactors of the indicated genes were derived from the SGD database
797 (https://www.yeastgenome.org/) (Cherry et al., 2012) and overlaid on a functional map based
798 on the global genetic interaction network of the yeast genome (Baryshnikova, 2016, Usaj et
799 al., 2017). *URA6* encodes an uridylate kinase essential for viability, which also exhibits
800 adenylate kinase activity.
801
802 Fig. S8 Simultaneous observation of Hsp104 and Pab1 foci
803 Wild-type cells expressing Hsp104-GFP and Pab1-RedStar2 were grown to the log phase at
804 37°C in medium containing 2% glucose. Cells were washed and released either in medium
805 containing 20 mM 2DG (top) or in medium lacking glucose (bottom), and then imaged after

806 30 and 60 min. White scale bar = 5 μm.

807

808 Fig. S9 Cytotoxicity of polyQ containing the huntingtin protein in wild-type and

809 ATP-mutant yeast cells

810 Each strain of the indicated genotype was transformed with an expression vector carrying

811 Htt103Q and grown on glucose ((-), no induction) or raffinose ((+), leaky expression) plates

812 at 30°C for 3 days.

813

814 Table S1. *Strains used in the present study*

Name	Genotype	Source	Figure
MTY3008	*snf1Δ::kanMX6 leu2Δ0 lys2Δ0 ura3Δ0*	Lab stock	1C, 3B, 5A-C, 5E, S9
MTY3015	*his3Δ1 leu2Δ0 lys2Δ0 ura3Δ0*	Lab stock	1C, 1F, 3B, 5A-E, S9
MTY3049	*adk1Δ::kanMX6 his3Δ1 leu2Δ0 lys2Δ0 ura3Δ0*	Lab stock	1C, 3B, 5A-E, S9
MTY3118	*bas1Δ::kanMX6 leu2Δ0 lys2Δ0 ura3Δ0*	Lab stock	1F, 3B, 5A-E, S9
MTY3143	*his3Δ1:: 2×pRS303-P_{TEF}-QUEEN-2m-T_{CYC1} leu2Δ0 lys2Δ0 ura3Δ0*	This study	S2
MTY3149	*adk1Δ::kanMX6 his3Δ1:: 2×pRS303-P_{TEF}-QUEEN-2m-T_{CYC1} leu2Δ0 lys2Δ0 ura3Δ0*	This study	S2
MTY3264	*his3Δ1:: 3×pRS303-P_{TEF}-QUEEN-2m-T_{CYC1} leu2Δ0 lys2Δ0 ura3Δ0 MYO1-3mCherry-hphMX6*	Takaine et al., 2019	1A-B, S1, S4
MTY3270	*bas1Δ::kanMX6 his3Δ1:: 3×pRS303-P_{TEF}-QUEEN-2m-T_{CYC1} leu2Δ0 lys2Δ0 ura3Δ0 MYO1-3mCherry-hphMX6*	This study	1D, 1E, 2E, S4, S6
MTY3293	*adk1Δ::kanMX6 his3Δ1:: 3×pRS303-P_{TEF}-QUEEN-2m-T_{CYC1} leu2Δ0 lys2Δ0 ura3Δ0 MYO1-3mCherry-hphMX6*	This study	1A-B
MTY3355	*adk1Δ::kanMX6 snf1Δ::natNT2 his3Δ1:: 3×pRS303-P_{TEF}-QUEEN-2m-T_{CYC1} leu2Δ0 lys2Δ0 ura3Δ0 MYO1-3mCherry-hphMX6*	This study	1A-B, 2A-D, S5
MTY3371	*snf1Δ::kanMX6 his3Δ1:: 3×pRS303-P_{TEF}-QUEEN-2m-T_{CYC1} leu2Δ0 lys2Δ0 ura3Δ0 MYO1-3mCherry-hphMX6*	This study	1A-B, S1, S4
MTY3412	*adk1Δ::kanMX6 snf1Δ::natNT2 leu2Δ0 lys2Δ0 ura3Δ0*	This study	1C, 3B, 5A-E, S9
MTY3417	*mig1Δ::natNT2 his3Δ1:: 3×pRS303-P_{TEF}-QUEEN-2m-T_{CYC1} leu2Δ0 lys2Δ0 ura3Δ0 MYO1-3mCherry-hphMX6*	This study	S1C
MTY3420	*Hsp104-yeGFP-hphNT1 his3Δ1 leu2Δ0 lys2Δ0 ura3Δ0*	This study	3C, D, 4A, B
MTY3421	*snf1Δ::kanMX6 Hsp104-yeGFP-hphNT1 his3Δ1 leu2Δ0 lys2Δ0 ura3Δ0*	This study	3C, D
MTY3422	*bas1Δ::kanMX6 Hsp104-yeGFP-hphNT1 his3Δ1 leu2Δ0 lys2Δ0 ura3Δ0*	This study	3C, D

MTY3424	*adk1Δ::kanMX6 Hsp104-yeGFP-hphNT1 his3Δ1 leu2Δ0 lys2Δ0 ura3Δ0*	This study	3C-D
MTY3425	*adk1Δ::kanMX6 snf1Δ::natNT2 Hsp104-yeGFP-hphNT1 his3Δ1 leu2Δ0 lys2Δ0 ura3Δ0*	This study	3C, D
MTY3489	*atg1Δ::kanMX6 his3Δ1 leu2Δ0 lys2Δ0 ura3Δ0*	Lab stock	5E
MTY3493	*snq2Δ::KILeu2; pdr3Δ::KIura3; pdr1Δ::natMX4; can1Δ::STE2prSp_his5 lyp1Δ his3Δ1 leu2Δ0 ura3Δ0 met15Δ0 LYS2+*	From Y. Ohya, (Piotrowski et al., 2017)	Parental strain of MTY3501
MTY3501	*Hsp104-yeGFP-hphNT1 snq2Δ::KILeu2; pdr3Δ::KIura3; pdr1Δ::natMX4; can1Δ::STE2prSp_his5 lyp1Δ his3Δ1 leu2Δ0 ura3Δ0 met15Δ0 LYS2+*	This study	5F
MTY3503	*Pab1- yeGFP-hphNT1 his3Δ1 leu2Δ0 lys2Δ0 ura3Δ0*	This study	3D
MTY3504	*Hsp104-yeGFP-hphNT1 Pab1-RedStar2-natNT2 his3Δ1 leu2Δ0 lys2Δ0 ura3Δ0*	This study	S8
MTY3505	*snf1Δ::kanMX6 Pab1- yeGFP-hphNT1 his3Δ1 leu2Δ0 lys2Δ0 ura3Δ0*	This study	3D
MTY3506	*adk1Δ::kanMX6 Pab1- yeGFP-hphNT1 his3Δ1 leu2Δ0 lys2Δ0 ura3Δ0*	This study	3D
MTY3507	*adk1Δ::kanMX6 snf1Δ::natNT2 Pab1- yeGFP-hphNT1 his3Δ1 leu2Δ0 lys2Δ0 ura3Δ0*	This study	3D
MTY3508	*bas1Δ::kanMX6 Pab1- yeGFP-hphNT1 his3Δ1 leu2Δ0 lys2Δ0 ura3Δ0*	This study	3D
MTY3513	*atg1Δ::natNT2 adk1Δ::kanMX6 his3Δ1 leu2Δ0 lys2Δ0 ura3Δ0*	This study	5E
MTY3514	*atg1Δ::natNT2 snf1Δ::kanMX6 his3Δ1 leu2Δ0 lys2Δ0 ura3Δ0*	This study	5E
MTY3515	*atg1Δ::natNT2 bas1Δ::kanMX6 his3Δ1 leu2Δ0 lys2Δ0 ura3Δ0*	This study	5E
MTY3516	*rpn4Δ::natNT2 adk1Δ::kanMX6 his3Δ1 leu2Δ0 lys2Δ0 ura3Δ0*	This study	5E
MTY3517	*rpn4Δ::natNT2 snf1Δ::kanMX6 his3Δ1 leu2Δ0 lys2Δ0 ura3Δ0*	This study	5E
MTY3518	*rpn4Δ::natNT2 bas1Δ::kanMX6 his3Δ1 leu2Δ0 lys2Δ0 ura3Δ0*	This study	5E
MTY3525	*rpn4Δ::kanMX6 his3Δ1 leu2Δ0 lys2Δ0 ura3Δ0*	Lab stock	5A-C, 5E

815

816 Table S2. *Plasmids used in the present study*

Name	Structure	Source	Purpose
MTP3091	pESC-Leu-GFP-Ubc9-ts	Judith Frydman (pJF1089)	Fig. 4C
MTP3088	p426 103Q GAL	Addgene (cat.# 1188)	Fig. S9
MTP3108	pYES2-α-synuclein-GFP	H. Takagi (Wijayanti et al., 2015)	Fig. 5A-D
MTP3090	pYES2-GFP	K. Ohashi	Fig. 5A

817 Captions for supplementary movies

818 **Movie S1**

819 Time-lapse imaging of QUEEN in *snf1*Δ*adk1*Δ cells in 2% glucose medium. Corresponding
820 to the data shown in Fig. 2A. The QUEEN ratio decreased twice (116 and 132 min) within a
821 short interval. White scale bar = 5 μm.

822

823 **Movie S2**

824 Another example of *snf1*Δ*adk1*Δ cells showing a sudden decrease in the QUEEN ratio.
825 Corresponding to the data shown in Fig. 2B. The QUEEN ratio decreased twice (180 and 356
826 min) with a long interval. White scale bar = 5 μm.

827

828 **Movie S3**

829 Oscillatory behavior of the QUEEN ratio in *bas1*Δ cells. Corresponding to the data shown in
830 Fig. 2E. Left, the QUEEN ratio image; middle, Myo1-mCherry (inverted grayscale image);
831 right, bright field image. Images were taken every 4 min. White scale bar = 5 μm.

832

833 **Movie S4**

834 Another example of *bas1*Δ cells showing an oscillating QUEEN ratio. Corresponding to the
835 data shown in Supplementary Fig. S6A. Left, the QUEEN ratio image; right, bright field
836 image. In this case, cytokinesis had already been completed at t = 0 min. Images were taken
837 every 3 min. White scale bar = 5 μm.

838

839

Fig. 1

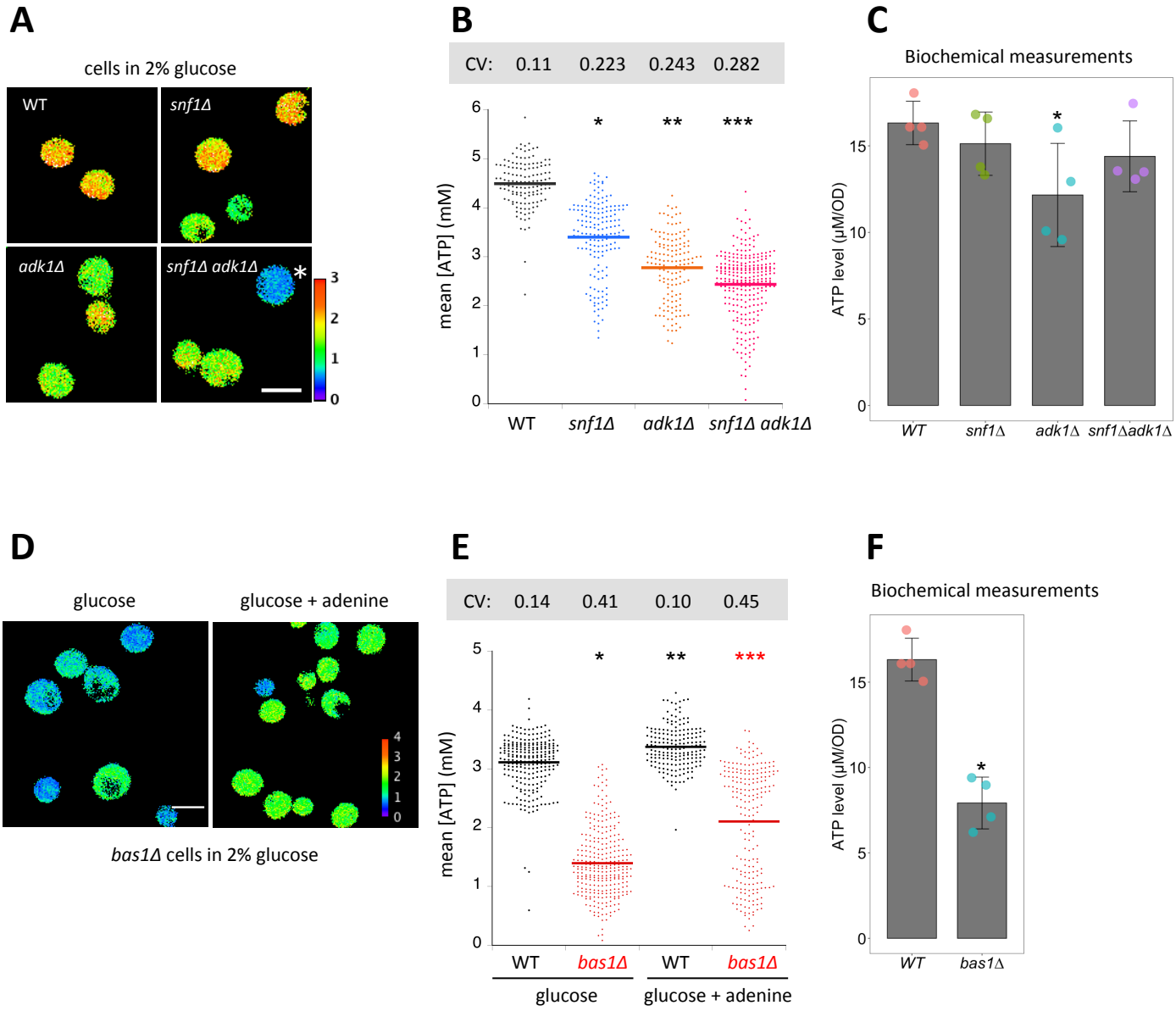
A
cells in 2% glucose
WT
snf1Δ
adk1Δ
snf1Δ adk1Δ
*
3
2
1
0
B
CV: 0.11 0.223 0.243 0.282
mean [ATP] (mM)
*
**
***
WT
snf1Δ
adk1Δ
snf1Δ adk1Δ
C
Biochemical measurements
ATP level (µM/OD)
*
WT
snf1Δ
adk1Δ
snf1Δadk1Δ
D
glucose
glucose + adenine
bas1Δ cells in 2% glucose
E
CV: 0.14 0.41 0.10 0.45
mean [ATP] (mM)
*
**
***
WT
bas1Δ
WT
bas1Δ
glucose
glucose + adenine
F
Biochemical measurements
ATP level (µM/OD)
*
WT
bas1Δ

Fig. 2

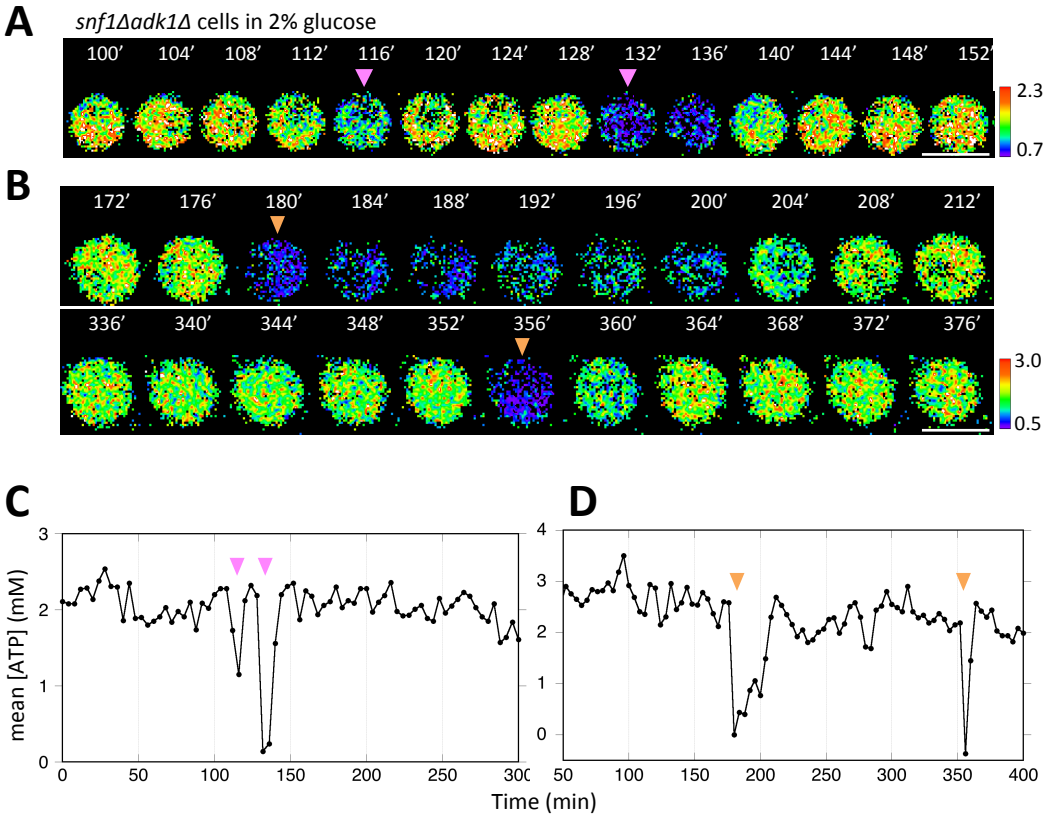
A
snf1Δadk1Δ cells in 2% glucose
100′ 104′ 108′ 112′ 116′ 120′ 124′ 128′ 132′ 136′ 140′ 144′ 148′ 152′
2.3
0.7
B
172′ 176′ 180′ 184′ 188′ 192′ 196′ 200′ 204′ 208′ 212′
336′ 340′ 344′ 348′ 352′ 356′ 360′ 364′ 368′ 372′ 376′
3.0
0.5
C
D
mean [ATP] (mM)
Time (min)

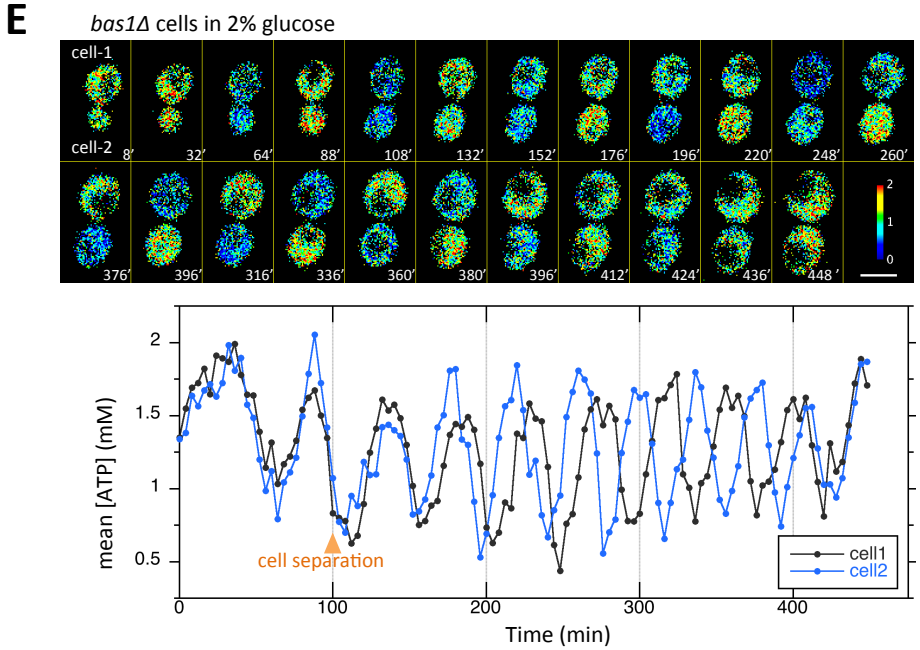
E
bas1Δ cells in 2% glucose
cell-1
cell-2
8′ 32′ 64′ 88′ 108′ 132′ 152′ 176′ 196′ 220′ 248′ 260′
376′ 396′ 316′ 336′ 360′ 380′ 396′ 412′ 424′ 436′ 448′
mean [ATP] (mM)
cell separation
cell1
cell2
Time (min)

Fig. 3

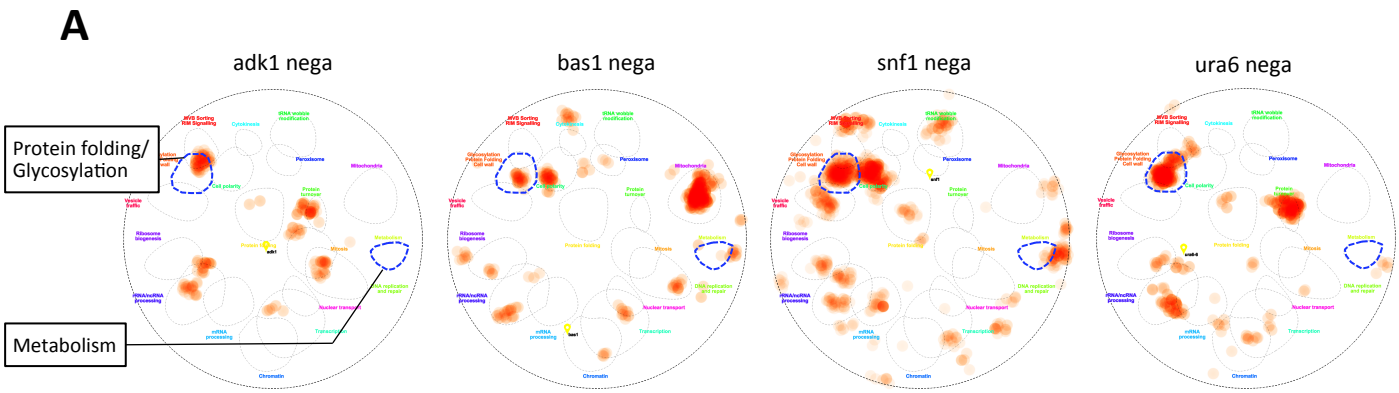
A
adk1 nega
bas1 nega
snf1 nega
ura6 nega
Protein folding/
Glycosylation
Metabolism

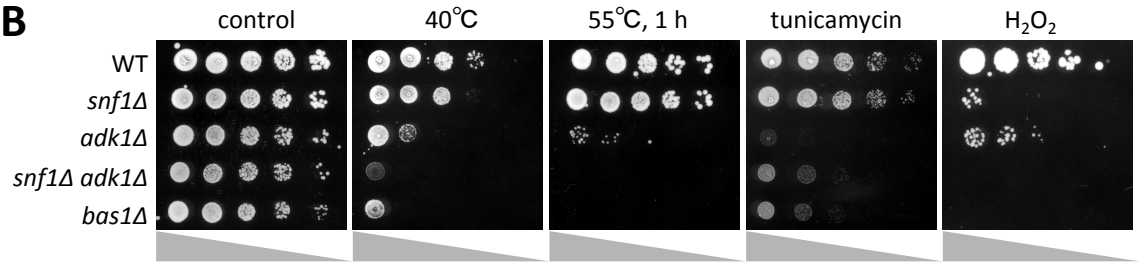
B
control
40°C
55°C, 1 h
tunicamycin
H2O2
WT
snf1Δ
adk1Δ
snf1Δ adk1Δ
bas1Δ

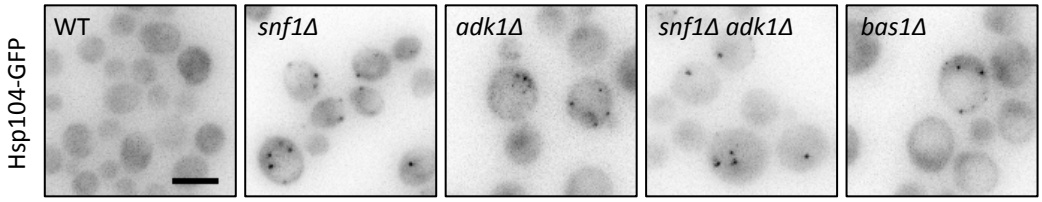
C
Hsp104-GFP
WT
snf1Δ
adk1Δ
snf1Δ adk1Δ
bas1Δ

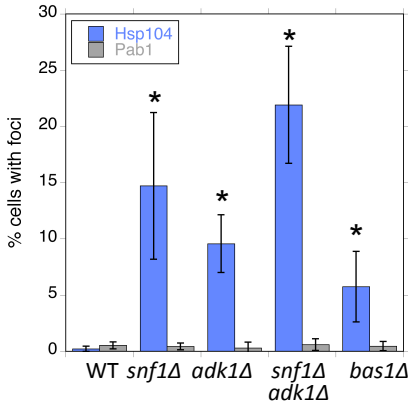
D
Hsp104
Pab1
% cells with foci
30
25
20
15
10
5
0
*
WT
snf1Δ
adk1Δ
snf1Δ adk1Δ
bas1Δ

Fig. 4

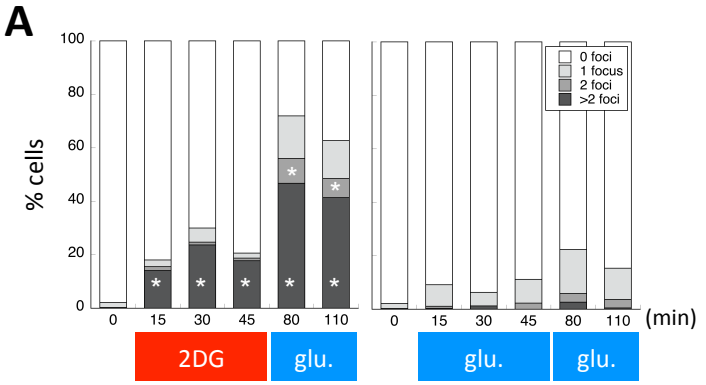
A
% cells
100
80
60
40
20
0
0 foci
1 focus
2 foci
>2 foci
0
15
30
45
80
110
(min)
2DG
glu.
glu.
glu.

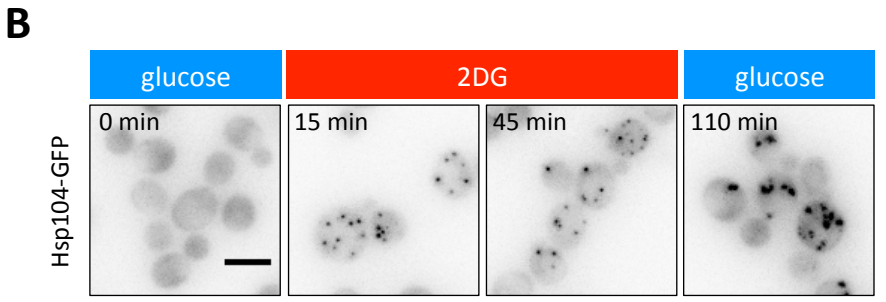
B
glucose
2DG
glucose
Hsp104-GFP
0 min
15 min
45 min
110 min

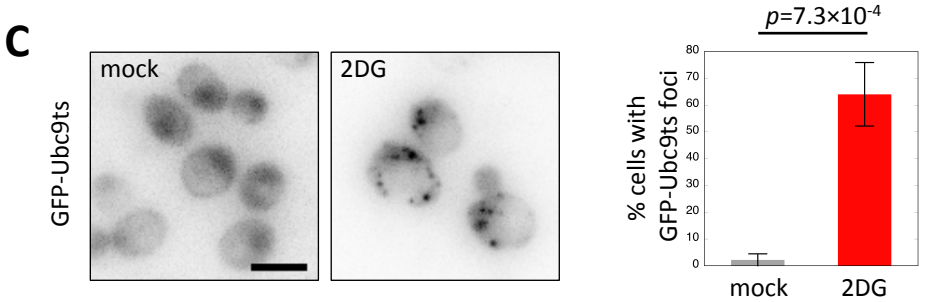
C
GFP-Ubc9ts
mock
2DG
p=7.3×10-4
% cells with GFP-Ubc9ts foci
80
70
60
50
40
30
20
10
0
mock
2DG

Fig. 5

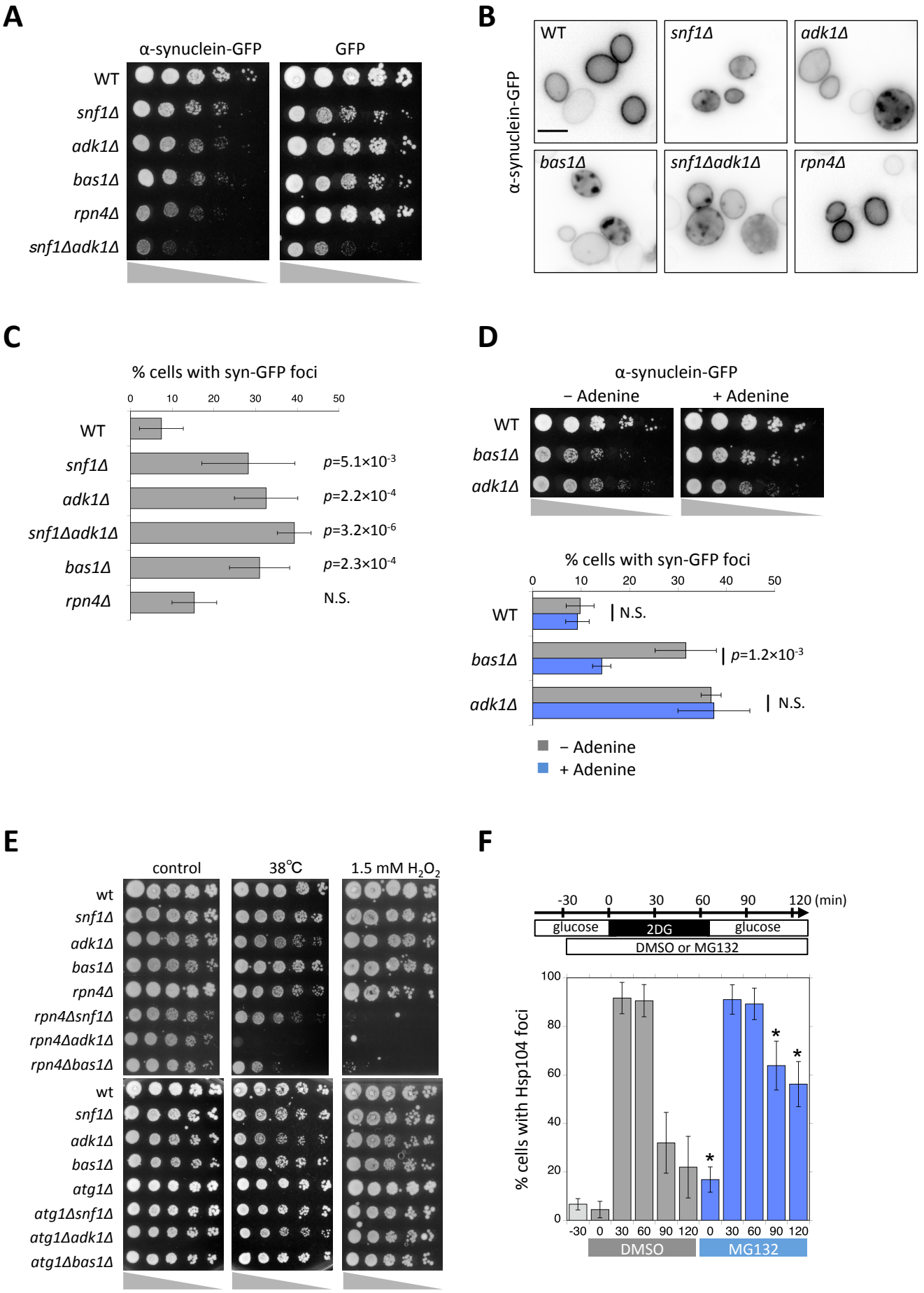
A
α-synuclein-GFP
GFP
WT
snf1Δ
adk1Δ
bas1Δ
rpn4Δ
snf1Δadk1Δ
B
α-synuclein-GFP
WT
snf1Δ
adk1Δ
bas1Δ
snf1Δadk1Δ
rpn4Δ
C
% cells with syn-GFP foci
0
10
20
30
40
50
WT
snf1Δ
adk1Δ
snf1Δadk1Δ
bas1Δ
rpn4Δ
p=5.1×10-3
p=2.2×10-4
p=3.2×10-6
p=2.3×10-4
N.S.
D
α-synuclein-GFP
− Adenine
+ Adenine
WT
bas1Δ
adk1Δ
% cells with syn-GFP foci
N.S.
p=1.2×10-3
N.S.
− Adenine
+ Adenine
E
control
38℃
1.5 mM H2O2
wt
snf1Δ
adk1Δ
bas1Δ
rpn4Δ
rpn4Δsnf1Δ
rpn4Δadk1Δ
rpn4Δbas1Δ
wt
snf1Δ
adk1Δ
bas1Δ
atg1Δ
atg1Δsnf1Δ
atg1Δadk1Δ
atg1Δbas1Δ
F
-30
0
30
60
90
120 (min)
glucose
2DG
glucose
DMSO or MG132
% cells with Hsp104 foci
100
80
60
40
20
0
-30 0 30 60 90 120 0 30 60 90 120
DMSO
MG132

Fig. 6

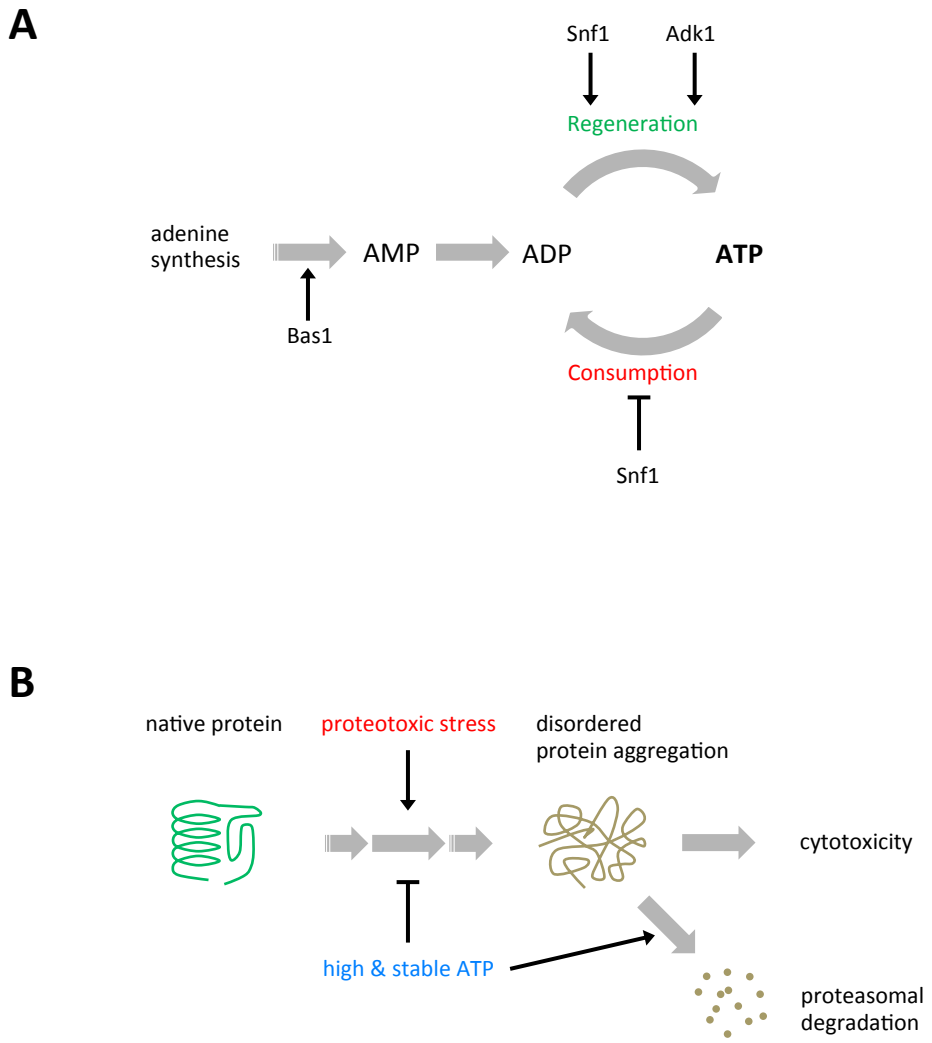
A
Snf1
Adk1
Regeneration
adenine synthesis
AMP
ADP
ATP
Bas1
Consumption
Snf1
B
native protein
proteotoxic stress
disordered protein aggregation
cytotoxicity
high & stable ATP
proteasomal degradation

Fig. S1

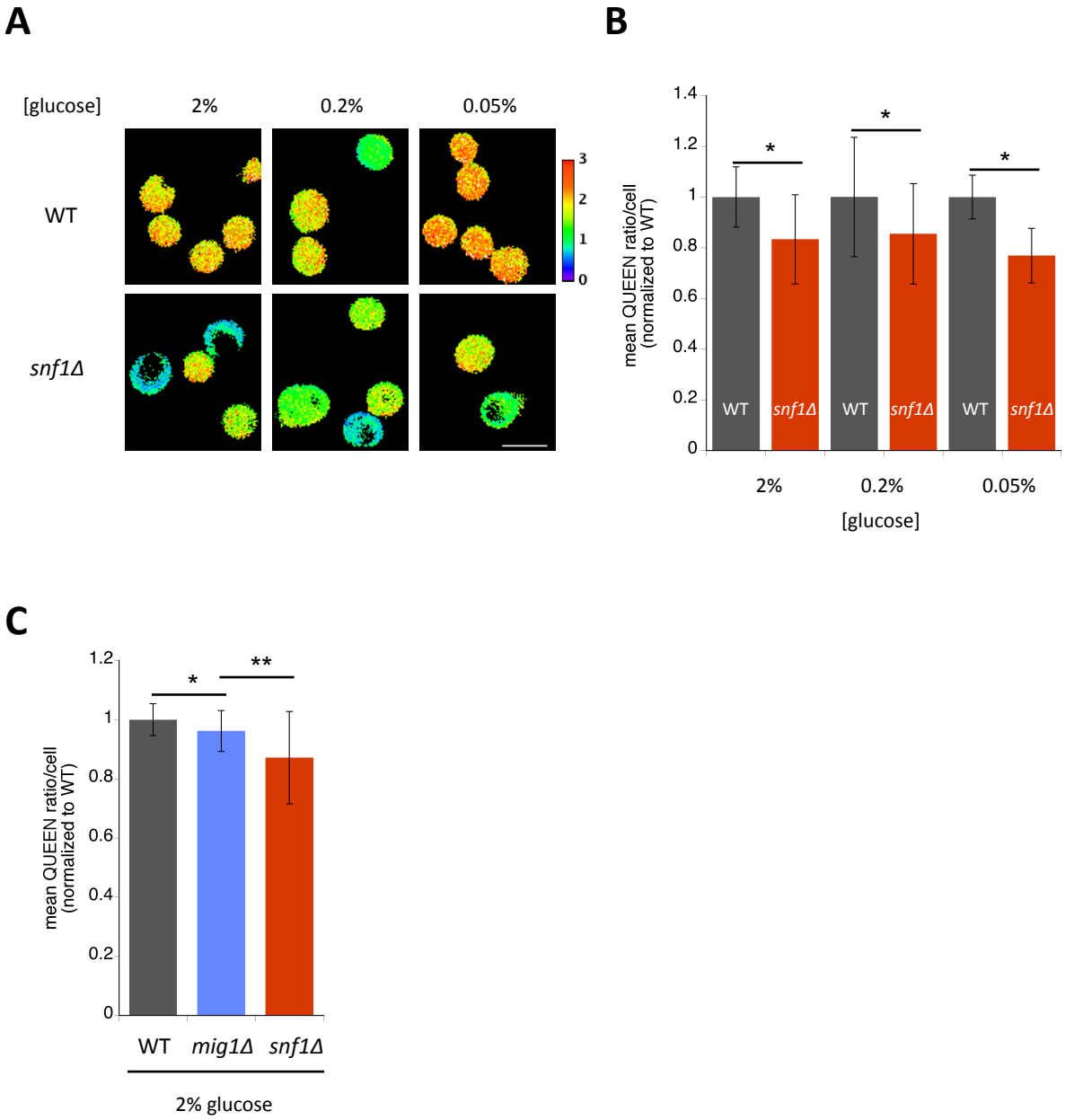
A
[glucose]
2%
0.2%
0.05%
WT
snf1Δ
3
2
1
0
B
mean QUEEN ratio/cell
(normalized to WT)
1.4
1.2
1
0.8
0.6
0.4
0.2
0
*
*
*
WT
snf1Δ
WT
snf1Δ
WT
snf1Δ
2%
0.2%
0.05%
[glucose]
C
mean QUEEN ratio/cell
(normalized to WT)
1.2
1
0.8
0.6
0.4
0.2
0
*
**
WT
mig1Δ
snf1Δ
2% glucose

Fig. S2

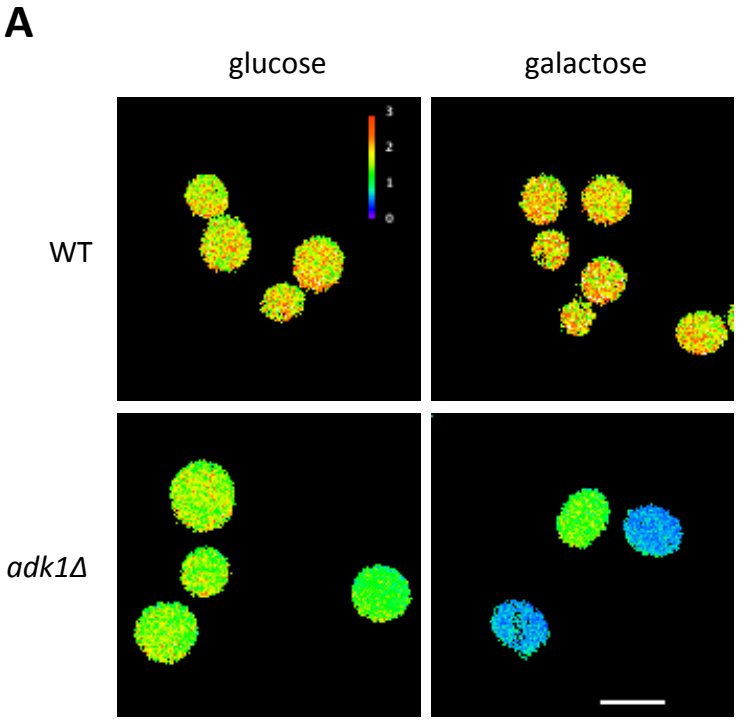
A
glucose
galactose
WT
adk1Δ
3
2
1
0

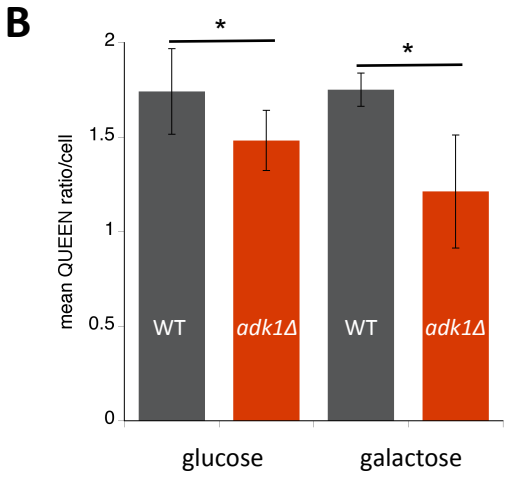
B
mean QUEEN ratio/cell
2
1.5
1
0.5
0
*
*
WT
adk1Δ
WT
adk1Δ
glucose
galactose

Fig. S3

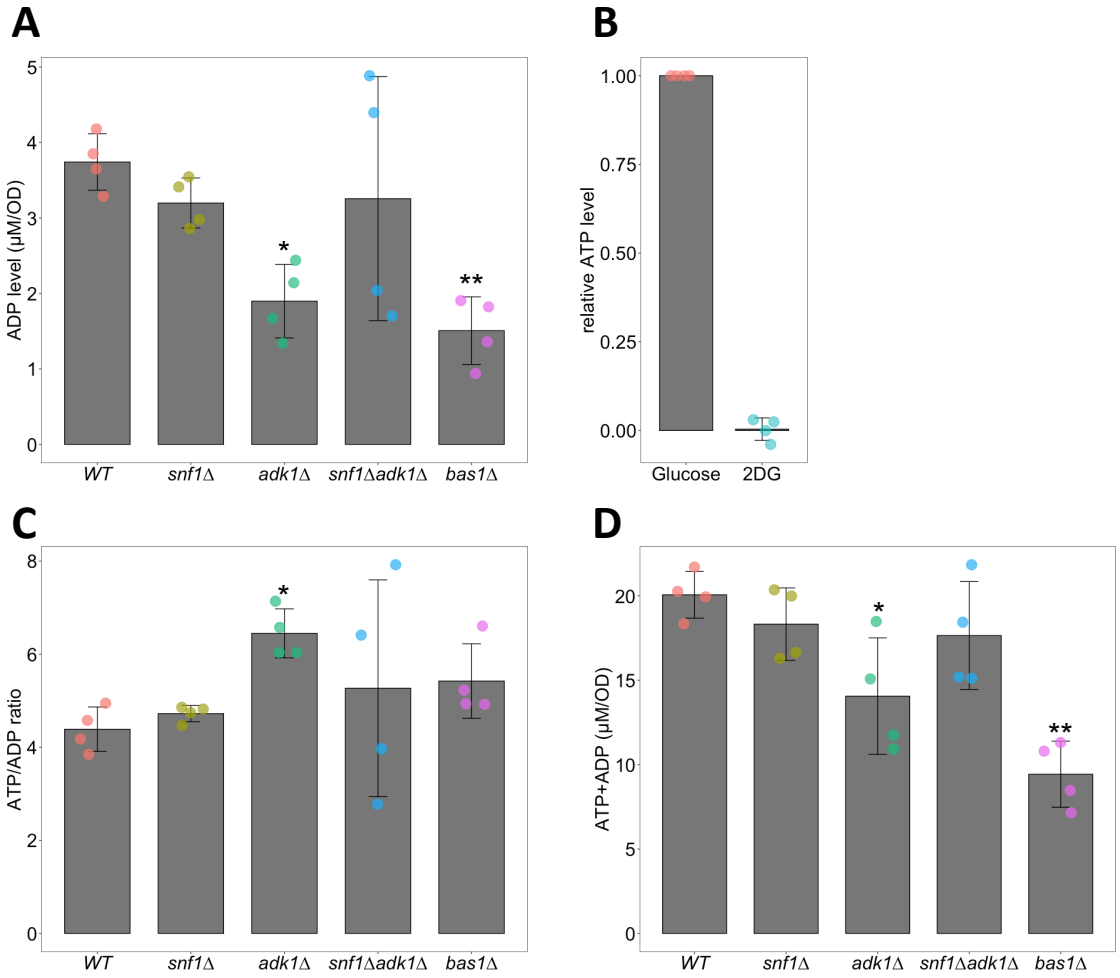
A
ADP level (μM/OD)
0
1
2
3
4
5
*
**
WT
snf1Δ
adk1Δ
snf1Δadk1Δ
bas1Δ
B
relative ATP level
0.00
0.25
0.50
0.75
1.00
Glucose
2DG
C
ATP/ADP ratio
0
2
4
6
8
*
WT
snf1Δ
adk1Δ
snf1Δadk1Δ
bas1Δ
D
ATP+ADP (μM/OD)
0
5
10
15
20
*
**
WT
snf1Δ
adk1Δ
snf1Δadk1Δ
bas1Δ

Fig. S4

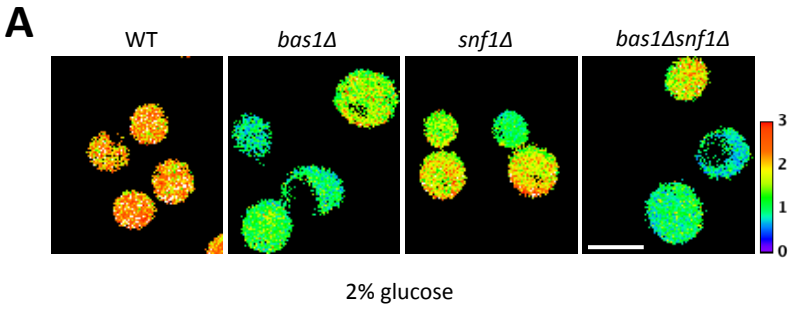
A
WT
bas1Δ
snf1Δ
bas1Δsnf1Δ
3
2
1
0
2% glucose

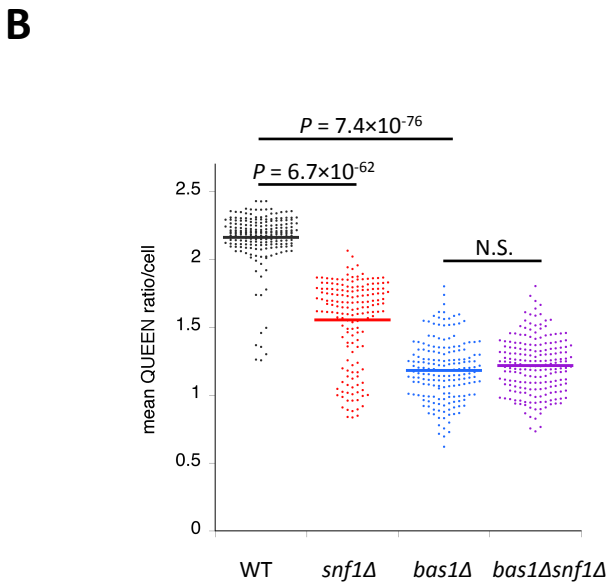
B
P = 7.4×10-76
P = 6.7×10-62
N.S.
mean QUEEN ratio/cell
2.5
2
1.5
1
0.5
0
WT
snf1Δ
bas1Δ
bas1Δsnf1Δ

Fig. S5

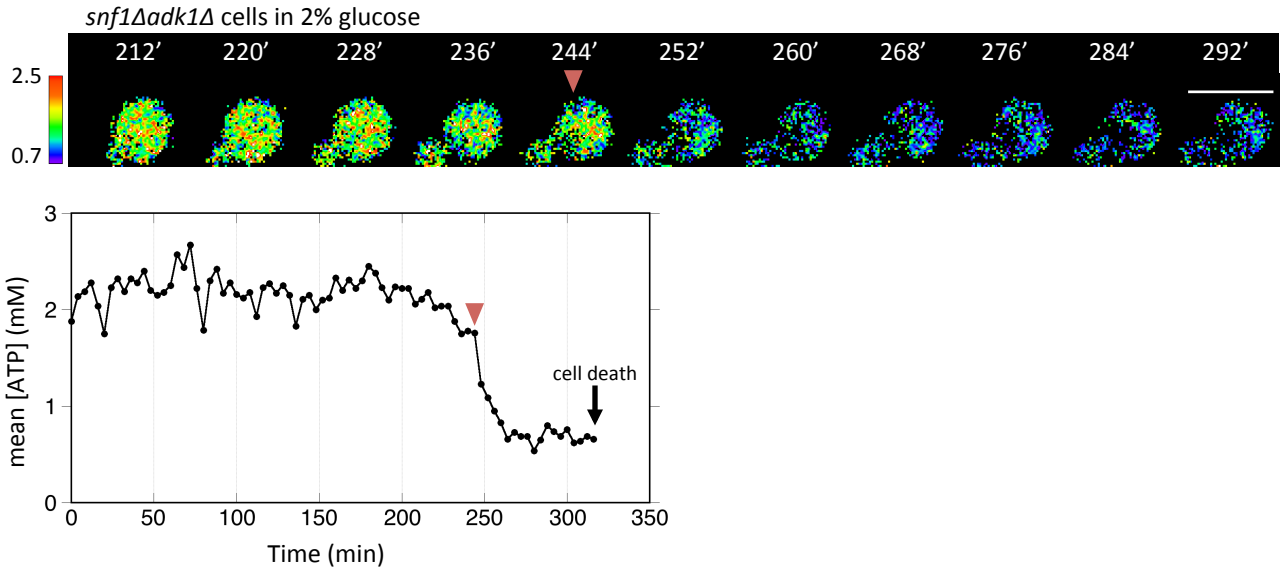
snf1Δadk1Δ cells in 2% glucose
212′
220′
228′
236′
244′
252′
260′
268′
276′
284′
292′
2.5
0.7
mean [ATP] (mM)
3
2
1
0
0
50
100
150
200
250
300
350
Time (min)
cell death

Fig. S6

A

bas1Δ cells in 2% glucose

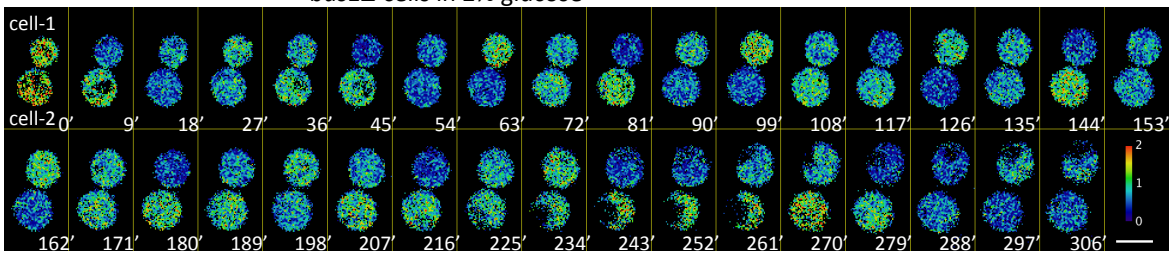

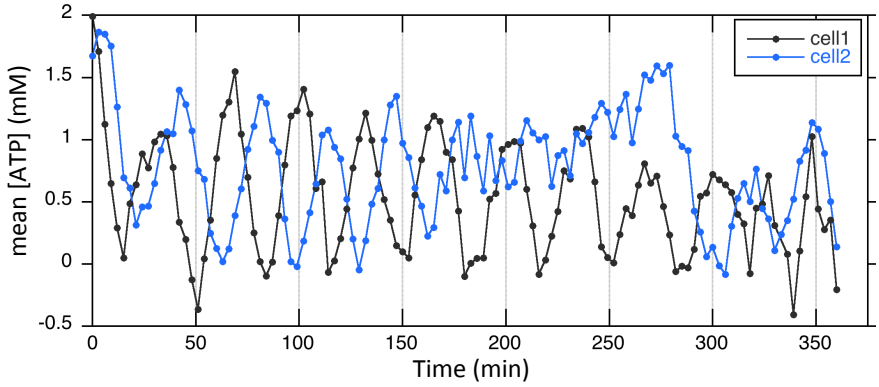

B

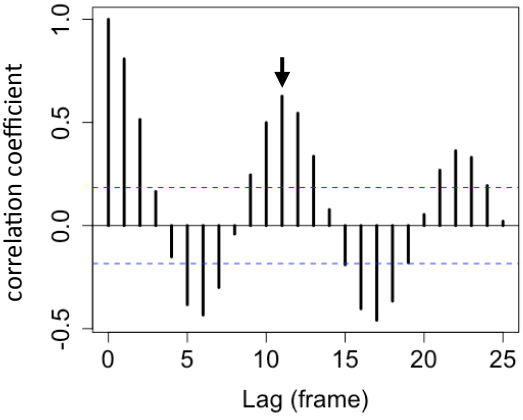

Fig. S7

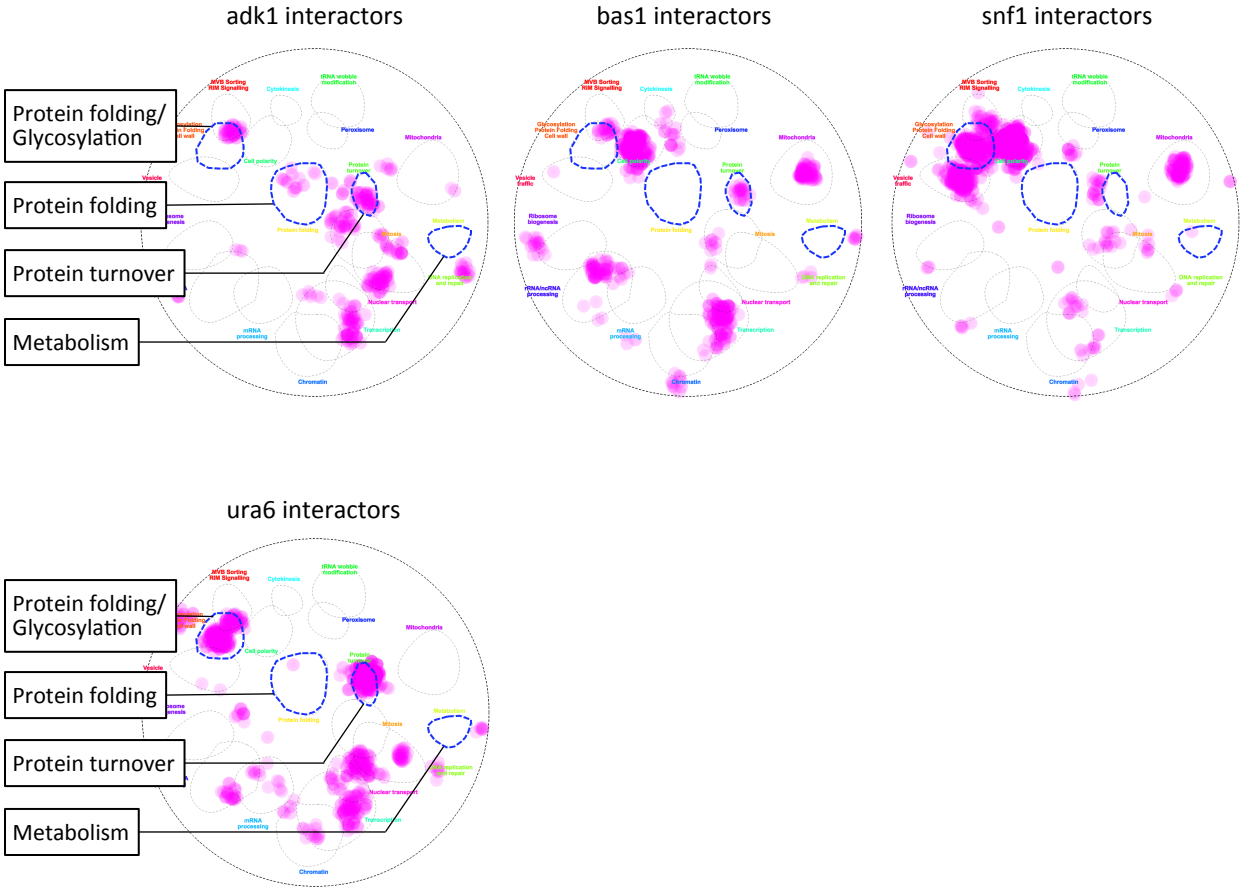
adk1 interactors
bas1 interactors
snf1 interactors
ura6 interactors
Protein folding/ Glycosylation
Protein folding
Protein turnover
Metabolism

Fig. S8

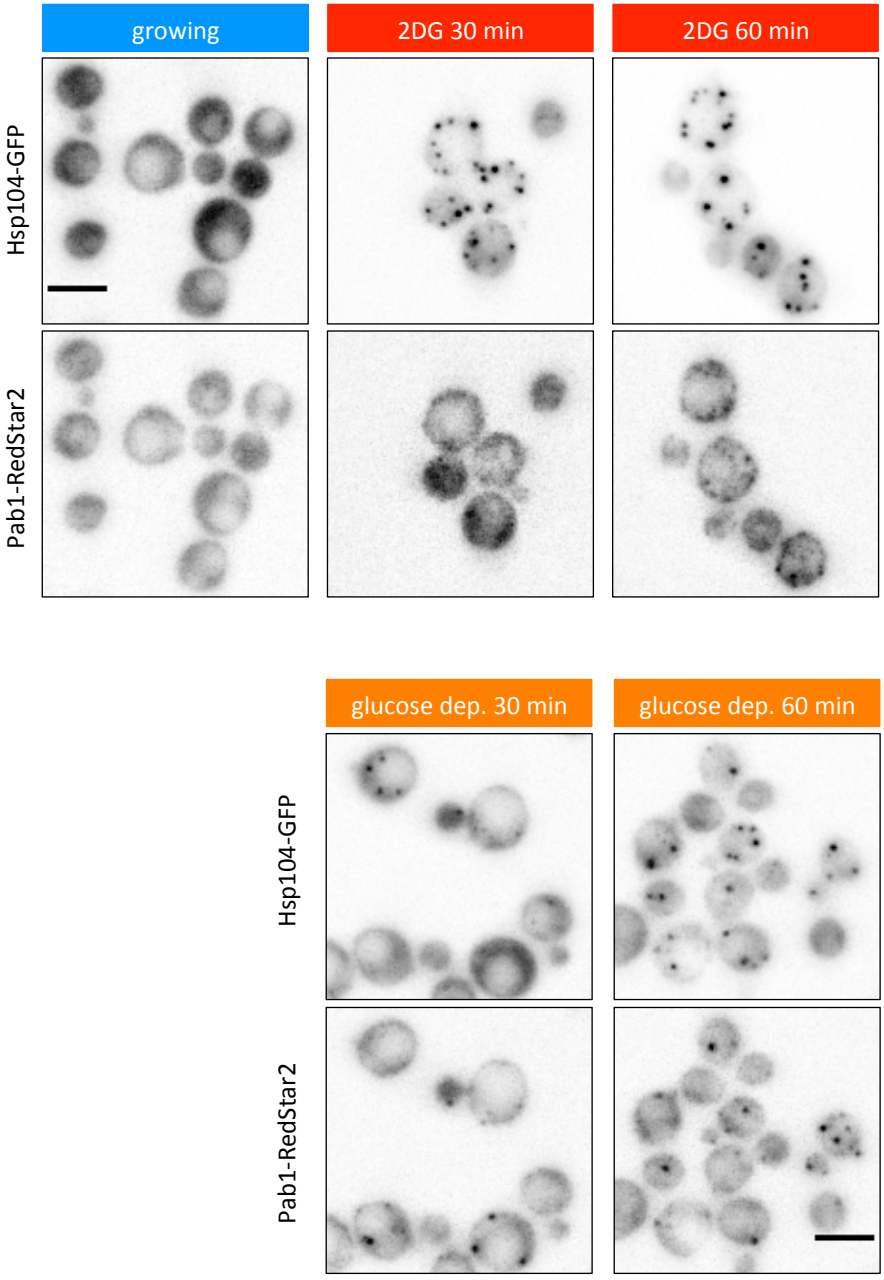
Hsp104-GFP
Pab1-RedStar2
growing
2DG 30 min
2DG 60 min
glucose dep. 30 min
glucose dep. 60 min
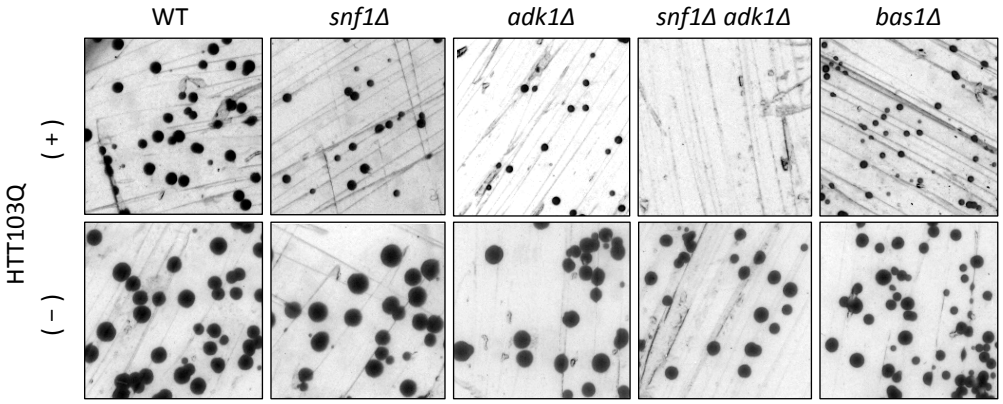
Fig. S9